Received Signal Strength-Based Localization of Non-Collaborative Emitters in the Presence of Correlated Shadowing

Ryan C. Taylor

Thesis submitted to the Faculty of the
Virginia Polytechnic Institute and State University
in partial fulfillment of the requirements for the degree of

Master of Science
in
Electrical Engineering

Robert W. McGwier, Chair
Aloysius A. Beex
Richard. M Buehrer

May 2, 2013
Blacksburg, Virginia

Keywords: Received Signal Strength, Differential Received Signal Strength, Localization, Cramér Rao Lower Bound, Correlated Shadowing

Received Signal Strength-Based Localization of Non-Collaborative Emitters in the Presence of Correlated Shadowing

Ryan C. Taylor

(ABSTRACT)

RSS-based localization is a promising solution for estimating the position of a non-collaborative emitter using a network of collaborative sensors. This paper examines RSS-based localization and differential RSS (DRSS) localization in the presence of correlated shadowing with no knowledge of the emitter's reference power. A new non-linear least squares (NLS) DRSS location estimator that uses correlated shadowing information to improve performance is introduced. The existing maximum likelihood (ML) estimator and Cramér Rao lower bound (CRLB) for RSS-based localization given do not account for correlated shadowing. This paper presents a new ML estimator and CRLB for RSS-based localization that account for spatially correlated shadowing and imperfect knowledge of the emitter's reference power. The performance of the ML estimator is compared to the CRLB under different simulation conditions. The ML estimator is shown to be biased when the number of sensors is small or the shadowing variance is large. The effects of correlated shadowing on an RSS-based location estimator are thoroughly examined. It is proven that an increase in correlated shadowing will improve the accuracy of an RSS-based location estimator. It is also demonstrated that the ideal sensor geometry which minimizes the average error becomes more compact as correlation is increased. A geometric dilution of precision (GDOP) formulation is derived that provides a metric for the effect of the position of the sensors and emitter on the location estimator performance.

A measurement campaign is conducted that characterizes the path loss at 3.4 GHz. The measurements are compared to the log-distance model. The errors between the model and the measurements, which should theoretically be Gaussian, have a Kurtosis value of 1.31. The errors were determined to be spatially correlated with an average correlation coefficient of 0.5 at a distance of 160 meters. The performance of the location estimators in simulation is compared to the performance using measurements from the measurement campaign. The performance is very similar, with the largest difference between the simulated and actual results in the ML estimator. In both cases, the new NLS DRSS estimator outperformed the other estimators and achieved the CRLB.

Contents

List of Figures

List of Tables

Chapter 1

Introduction

1.1 Background

With the growing demand for wireless capacity, there is a need for systems that opportunistically seek out free spectrum. To do this while reducing interference, these radio systems rely on radio environment maps (REMs), which characterize the surrounding radio emitters. An important element of any REM is the classification of the neighboring radio emitters' geographic positions. Specially designed radio systems may have the ability to identify their own position via systems like the Global Positioning System (GPS) and then communicate it to the REM, but this functionality is not an option for the legacy systems that these systems are attempting to avoid. A specific need for this geographic positioning arose in 2010 when the Federal Communications Commission (FCC) released a memorandum that allows secondary users to opportunistically use spectrum not occupied by certain licensed primary users [6]. The primary users are required to report their geographic position to a REM, which secondary users can then access to ensure they will not interfere. There is no process for secondary users to report their position to the REM, so in order to reduce interference among secondary users, a secondary user must determine the geographic position of neighboring secondary users.

1.2 Defining the Problem

As stated in Section 1.1, there exists a need to identify the location of non-collaborative emitters, that is, emitters that cannot or will not identify their own location and/or communicate it to a REM. These emitters may be legacy communication systems in an area of cognitive radios or emitters intentionally interfering with neighboring systems (jammers). To solve this problem, it is assumed that there exists a network of collaborative sensing

nodes that can exchange information. It is assumed the locations of these sensing nodes, referred to as sensors, are known. Additionally, the frequency and bandwidth of the emitter are known or readily detectable by all sensors. To maximize the application of the solution, it is further assumed the sensors may be a diverse set of transceivers. The only required functionality is the ability to determine the received signal strength (RSS) at the emitter's transmit frequency and bandwidth. The ability to determine RSS is a feature built into nearly all transceivers and is typically referred to as the received signal strength indicator (RSSI). An extensive list of the assumptions and constraints on the solution are listed below. They are intended to maximize the scope of the application and reduce the complexity and cost of the solution.

Assumptions and Constraints

1. There exists a network of collaborative sensing nodes with known positions and known antenna patterns.
2. Sensors may be an identical or diverse set of transceivers.
3. Sensors may primarily serve purposes other than position location (e.g., WiFi, cellular communications). Position location may be a secondary function.
4. Sensors have the ability to measure received signal strength at the frequency and bandwidth of the emitter.
5. Bandwidth and frequency of the emitter are known or readily detectable parameters.
6. The emitter has an omni-directional antenna pattern.
7. Synchronization of internal clocks across network of sensors is not possible.
8. Signals from the emitter may be highly autocorrelated.
9. Perfect association of the received signal with the signal from emitter is possible, for example, co-channel signals do not exist or can be mitigated.

1.3 Motivation for RSS-Based Localization

There are many well-documented methods for solving the proposed problem. But based on the constraints and assumptions, RSS-based positioning is the most promising avenue of research. RSS-based positioning requires simple hardware and low network overhead. It is a solution that ensures the broadest range of transceivers can be used. Ideally, an RSS-based

solution to the proposed problem could be implemented on existing infrastructure with no modification to hardware and very little modification to the software.

Other positioning methods include time of arrival (TOA), time difference of arrival (TDOA), and angle of arrival (AOA). TDOA and TOA require more network bandwidth than RSS-based methods, and in the case of AOA, require additional hardware elements. In simulation and experimental analysis, RSS-based positioning systems generally perform worse in terms of root mean-squared distance error (RMSE) than positioning systems based on TOA, TDOA, and AOA. Despite the coarse accuracy of RSS-based positioning, it may be the only viable solution to the problem because of the following:

1. TOA is not a viable solution because *a priori* knowledge of the phase or amplitude of the transmitted signal is required to ascertain the time of flight. If this information is not available, *a priori* knowledge of the transmit time is required.

2. TDOA does not require *a priori* knowledge of the transmitted signal, but it does require the sampling clocks on all of the sensors to be synchronized. TDOA also requires the transmitted signal to not be autocorrelated. For instance, a narrow-band analog AM or FM voice signal does not exhibit sufficient autocorrelation properties to provide time resolution for TOA or TDOA algorithms. TDOA has been used to identify the location of non-collaborative nodes, most notably in the Uplink-TDOA system implemented on cellular networks [30]. The Uplink-TDOA is used to locate cellular handsets to allow cellular providers to comply with the E-911 standard. In this case, expensive synchronization equipment at each cellular base station is required to determine the offset of the internal clocks on all base station receivers. The use of expensive synchronization equipment at each sensor is not a viable solution for the proposed problem. It may be possible to synchronize the clocks of sensors with the aid of GPS, but this solution then precludes the use of indoor sensor nodes where the GPS signal cannot be received. Additionally, TDOA requires all samples from the received signal to be communicated over the network for processing at a central node.

3. AOA positioning systems require knowledge of the angle of the incoming signal from the non-collaborative emitter. The angle of arrival is obtained from an antenna array or multiple directional antennas on the receiver. This added complexity precludes most legacy receivers from the solution. Also, AOA is highly susceptible to multipath signals. If there is no line-of-sight path or the line-of-sight path is weaker than the multipath, the estimated AOA will be in error.

RSS-based positioning is the most suitable solution because it does not require internal clocks to be synchronized, it does not rely on specialized hardware, it requires relatively

small network bandwidth compared to TOA and TDOA, and there are no constraints on the signal's autocorrelation.

1.4 Focus of Work

The main focus of this work is on furthering the understanding of RSS-based localization methods in the presence of correlated shadowing. The existing maximum likelihood (ML) estimator and Cramér Rao lower bound (CRLB) for RSS-based localization given in [32] do not account for correlated shadowing. A CRLB that accounts for spatially correlated shadowing is given in [17], but it does not account for imperfect knowledge of the emitter's reference power. This paper presents a new ML estimator and CRLB that account for spatially correlated shadowing and imperfect knowledge of the reference power. The performance of the ML estimator is compared to the CRLB under different simulation conditions. New insight on the effects of correlation on the CRLB is presented. A geometric dilution of precision (GDOP) formulation is derived that provides a metric for the effect of the position of the sensors and emitter on the location estimator performance. This GDOP formulation is used to compare several sensor geometries and how they behave under different levels of correlated shadowing.

This paper also focuses on differential RSS (DRSS) localization. Source [32] proves the ML estimator and CRLB for DRSS localization and RSS localization are identical in the presence of no correlated shadowing. This paper further shows DRSS and RSS localization estimators provide identical results in the presence of correlated shadowing. Additionally, two new DRSS objective functions are presented and compared to the ML estimator.

Finally, a measurement campaign is conducted to obtain an actual set of RSS measurements. Most publications rely on simulations to test location estimators, but the measurements from the campaign show the performance of the location estimators under real-world conditions. The measurements are also used to verify the statistical log-normal shadowing model and a spatially correlated shadowing model.

1.5 Overview of Thesis

Chapter 2: Review of RSS-Based Localization

Chapter 2 provides a review of the underlying theory of RSS-based localization. This includes deterministic and statistical models used for predicting RSS at a given distance from an emitter. Explanations are provided for the sources of error in RSS-based localization, which include shadowing, multipath, path loss exponent, noise, geometric configuration, measurement noise, and antenna orientation. Existing RSS-based localization techniques

are presented with the main focus on RSS lateration. The non-linear least squares formulation of RSS lateration is presented.

Chapter 3: Review of Differential RSS

Chapter 3 describes DRSS localization and its theory. A geometric explanation is given for the ranging circles formed by DRSS. Previous work on DRSS localization is reviewed, which includes the derivation of the ML estimator and the CRLB assuming shadowing is not correlated.

Chapter 4: Solving NLSD and NLSR

Chapter 4 explains the method used for generating simulated RSS values and the method for solving the non-linear objective functions. The fminsearch function in Matlab is used to evaluate all objective functions. RSS values are simulated based on the log-normal shadowing model. The NLSD and NLSR estimators are compared in simulation and found to perform identically even as the correlated shadowing increases.

Chapter 5: ML Estimator and CRLB

Chapter 5 provides the existing ML estimator and CRLB for RSS-based localization. A new ML estimator and CRLB are presented for RSS-based localization in the presence of the spatially correlated shadowing. The ML estimator is compared to the CRLB and shown to be biased when the number of sensors is low or the shadowing variance is high. The effect of sensor geometry on the average miss distance is evaluated using the CRLB. It is shown that the ideal geometric configuration changes as correlation is increased. The optimal sensor configuration tends to be more compact as the spatial correlation increases.

Chapter 6: New Objective Function

Chapter 6 presents a new objective function that seeks to improve the performance of DRSS localization. The residuals of the objective functions are weighted by the correlation of the respective DRSS pairs. The objective function is compared to the RSS-based ML estimator and standard DRSS estimator in simulation. In nearly all cases, the new objective function slightly outperforms the standard DRSS estimator, but not the RSS-based ML estimator. The new objective function outperforms the RSS-based ML estimator when the correlation is low and the sensor configuration is such that the emitter is positioned at the center of a square bounding box and the sensors are randomly placed within that box.

Chapter 7: Measurement Campaign

Chapter 7 describes the method and results of the measurement campaign. The measurement campaign is conducted to obtain a set of actual RSS values that can be used to evaluate the localization estimators discussed in this paper. The measurements are compared to the log-distance model and the variance of the errors is found to be 69.54 dB. The mean of the errors is 0.12 dB and the distance at which correlation of the errors drops to 0.5 is 160 meters. Using the chi-square goodness-of-fit test, the null hypothesis that the errors are a random sample from a normal distribution, is rejected at the 99% significance level. The Kurtosis value of the errors is determined to be 1.31.

Chapter 8: Experimental Evaluation of Location Estimators

Chapter 8 provides new insight into the performance of the localization estimators by evaluating them using actual RSS values. The performance of the estimators based on actual RSS is compared to estimators based on simulated RSS. The performance is found to be very similar. The estimator with the lowest average miss distance is the new DRSS estimator proposed in Chapter 6.

Chapter 2

Review of RSS-Based Localization

2.1 Modeling RSS

Localization methods based on RSS generally use the distance between the emitter and sensor as a primary measurement for determining position. This is obtained from a model describing the relationship between RSS and distance. The model most often used in publication is the Friis Transmission formula [1].

$$\Omega_k = P_t + G_t + G_r + 10\alpha \log_{10}\left(\frac{\lambda}{4\pi d_k}\right) \tag{2.1}$$

where Ω_k is the received power, P_t is the transmit power, G_t is the transmit gain, G_r is the received gain, α is the path loss exponent, and d_k is the propagation distance. If P_r is known at a close in location to the transmitter, Friis formula can be simplified to the log distance path loss model. In this model, the relationship between distance and RSS is a follows [23]:

$$\Omega_k = c - 10\alpha \log_{10}\left(\frac{d_k}{d_0}\right) \tag{2.2}$$

where Ω_k is the received power at distance d_k, c is the power received at a close distance d_0, and α is a constant path loss value. Under ideal, LOS conditions, the value of α is 2, but in practice the value can range from 2 to 6. In this paper, d_0 is assumed to be 1 meter unless stated otherwise. The distance d_k is defined as the Euclidean distance between the emitter position (x, y) and the receiver position (x_k, y_k),

$$d_k = \sqrt{(x - x_k)^2 + (y - y_k)^2} \tag{2.3}$$

The log distance model is often used as a statistical model that accounts for the effects of shadowing. In this case, it is called the log normal shadowing model,

$$\Omega_k = c - 10\alpha log_{10}\left(\frac{d_k}{d_0}\right) + X_k \tag{2.4}$$

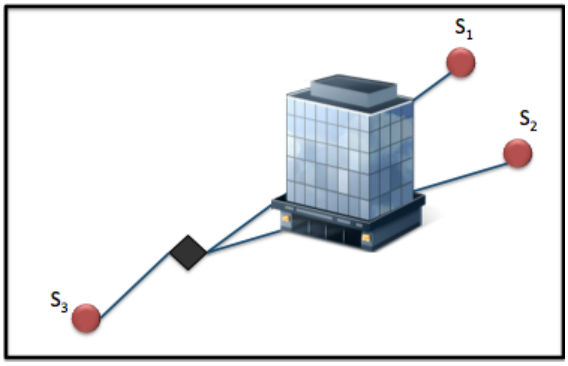

Figure 2.1: Spatially Correlated Shadowing Diagram: Correlation between the shadowing variables for two sensors is dependent upon their proximity. The random shadowing experienced at each of the three sensors (circles) from the emitter (square) will be different. In this example, the shadowing variables for sensors S_1 and S_2 will be more correlated than S_1 and S_3 or S_2 and S_3.

where X_k represents the effects of shadowing and is a zero mean Gaussian random variable with a variance σ_k^2. This variance of the shadowing variable has been modeled as a function of the distance from the emitter, but in this paper it is assumed to be a constant. The correlation between random variables X_k and X_j is defined by the correlation matrix $\mathbf{\Gamma}$. One model for this correlation is given in [34] where the correlation is dependent upon the distance between the two receiving sensors. The off-diagonal element (i, j) of $\mathbf{\Gamma}$ is defined as follows:

$$\Gamma_{(i,j)} = \sigma_x^2 \exp\left(-\frac{d_{ij}}{d_{corr}} \ln(2)\right), \quad i \neq j \tag{2.5}$$

where d_{ij} is the distance between sensors i and j, and d_{corr} is a constant correlation distance, which is based on the distance at which the correlation, ρ, drops to 0.5. The diagonal elements of $\mathbf{\Gamma}$ are $diag(\sigma_x^2)$. This model is used exclusively for the covariance matrix in this paper. Based on this, the correlation between any two sensors i and j is as follows:

$$\rho_{(i,j)} = \exp\left(-\frac{d_{ij}}{d_{corr}} \ln(2)\right) \tag{2.6}$$

Correlation dependent on distance is assumed to exist because sensors that are close in distance will likely have similar channels to the emitter. Fig. 2.1 illustrates the similar path losses experienced by two sensors close in proximity. In [35] and [16], the shadowing experienced at separate receivers is shown to be spatially correlated with correlation coefficients as high as 0.2 for indoor and 0.8 for outdoor.

2.2 Sources of Localization Error

RSS-based localization is challenging because there are numerous factors affecting the energy decay between the transmitter and emitter. These factors include shadowing, multipath, path loss exponent estimation errors, noise, geometric configuration of the nodes, measurement error, and antenna orientation. All of these have an effect on the performance of RSS-based estimators.

Shadowing

Path loss caused by the absorption of signals by obstructions between the emitter and receiver such as trees, buildings, or mountains is known as shadowing, or large scale fading. The effects of shadowing are nearly impossible to predict in a deterministic fashion so they most often are modeled statistically as a zero mean Gaussian random variable on the dB scale [23].

Multipath

Multipath occurs when multiple signal components combine either constructively or destructively at the receiver. This can occur when a LOS component combines with a non-line-of-sight (NLOS) component. NLOS components are caused by reflections, refractions, and diffractions in the channel. Rice and Rayleigh are statistical models for multipath that characterize the envelope of an incoming signal. Unlike shadowing, the multipath experienced at two different sensors is typically assumed to be uncorrelated. Multipath causes rapid changes in the RSS that are generally smaller in magnitude than shadowing.

Path Loss Exponent

The pass loss exponent (PLE) α, defines the rate at which the signal power decays over distance. Errors can result when there is imperfect knowledge of the PLE. If there is no knowledge of PLE, it must be estimated, which makes the localization problem more difficult [27]. The percent error in the PLE is equivalent to the percent error in the range assuming the log distance path loss model in Eqn. 7.1. The value of the PLE can have a significant impact on the performance of a location estimator. As shown in Chapter 5, the RMSE performance of an RSS-based estimator improves as the PLE increases.

Noise

Noise occurs when unwanted energy is in the spectrum band of interest. This could be naturally occurring environmental noise, noise from the receiver components, or noise from co-channel interference sources. If the additional energy received by the receiver cannot be filtered, it will distort the RSS measurement. In this paper, it is assumed that co-channel interference from other transmitters can either be filtered or does not exist.

Geometric Configuration

The effect the position of the sensors and emitter has on the accuracy of the localization result is called geometric dilution of precision (GDOP). This phenomonon is discussed in

detail in Chapter 5.

Measurement Error

RSS measurement errors will cause errors in the localization. For instance, if the sensor has an RSS resolution of 5 dB and $\alpha = 2$, the range will be off by as much as 77 percent.

Antenna Orientation

In this paper, it is assumed an emitter has an omnidirectional antenna pattern such that the received power at all angles in the horizontal plane is equal. In practice, most omnidirectional antennas are not perfectly omnidirectional in the horizontal plane and, more importantly, are only designed to be omnidirectional in one plane. Therefore the orientation of an antenna significantly impacts the gain in a given direction. Experimental analysis performed in [4] shows that RSS can vary by a factor of 5 depending on antenna orientation and optimally calibrated RSS localization performance can decrease by 32%. The effects of antenna orientation are mitigated in [33] with the aid of accelerometers on the emitter to determine orientation.

2.3 RSS-Based Localization Techniques

This section reviews some of the proposed RSS-based positioning methods. The methods are designated as range based and range free. Range-based methods use RSS as a reference for distance, and range-free methods do not use distances or ranges. DRSS is reviewed in Chapter 3.

2.3.1 Range Based

RSS Lateration

The coordinates of a point can be defined solely by ranges to a set of known coordinates. For the localization of one point in 2-dimensions, three ranges are required. Fig. 2.2 illustrates the concept of lateration with three ranging circles intersecting at a single point. One range creates a circle centered at the respective known coordinates, and a set of three range circles centered at three known coordinates intersect at the coordinates of a single point. This concept of positioning is widely used, most notably in the GPS. The relationship between the ranges and the known positions (sensors) and unknown position (emitter) is given by the following system of non-linear equations:

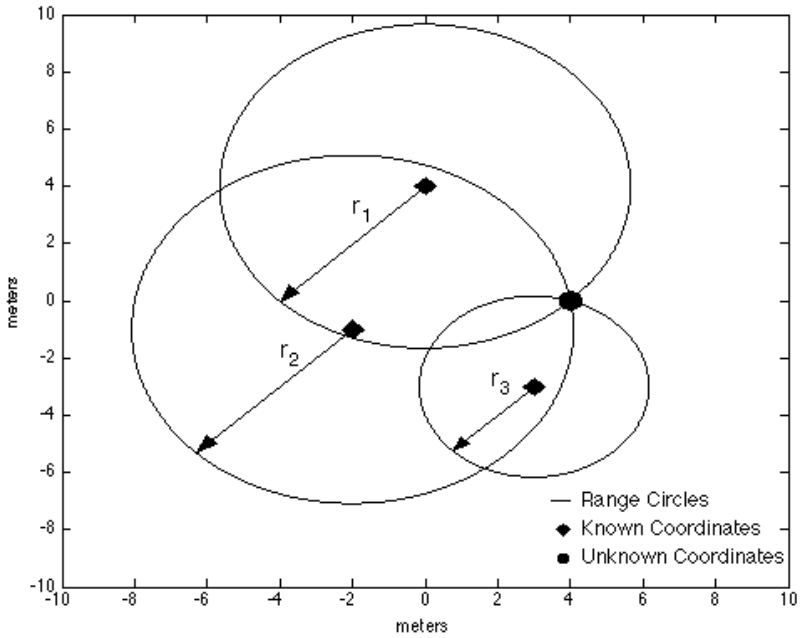

Figure 2.2: Lateration with Perfect Range Estimates

$$\begin{aligned} r_1 &= \sqrt{(x-x_1)^2 + (y-y_1)^2} \\ r_2 &= \sqrt{(x-x_2)^2 + (y-y_2)^2} \\ r_3 &= \sqrt{(x-x_3)^2 + (y-y_3)^2} \end{aligned} \tag{2.7}$$

where r_i is the range to sensor i, (x,y) is the emitter's position, and (x_i,y_i) is the position of sensor i.

As noted in Section 2.2, RSS measurements are corrupted by several factors that cause errors in the resulting range estimate. These range errors cause ambiguity in the range circles intersection point as shown in Fig. 2.3. The most common method for solving is the least squares formulation. Least squares seeks to minimize the square error between the observed and the predicted ranges. In this case the optimization is as follows:

$$\hat{\boldsymbol{\theta}} = \arg\min_{\boldsymbol{\theta}} \sum_{i=1}^{N} \left(10^{\frac{\Omega_i + c}{10\alpha}} - r_i \right)^2 \tag{2.8}$$

where $\boldsymbol{\theta} = [x, y, c]$ is the emitter position and reference power, r_i is the distance from sensor i to the emitter, Ω_i is the power received by sensor i, and N is the number of sensors. This is

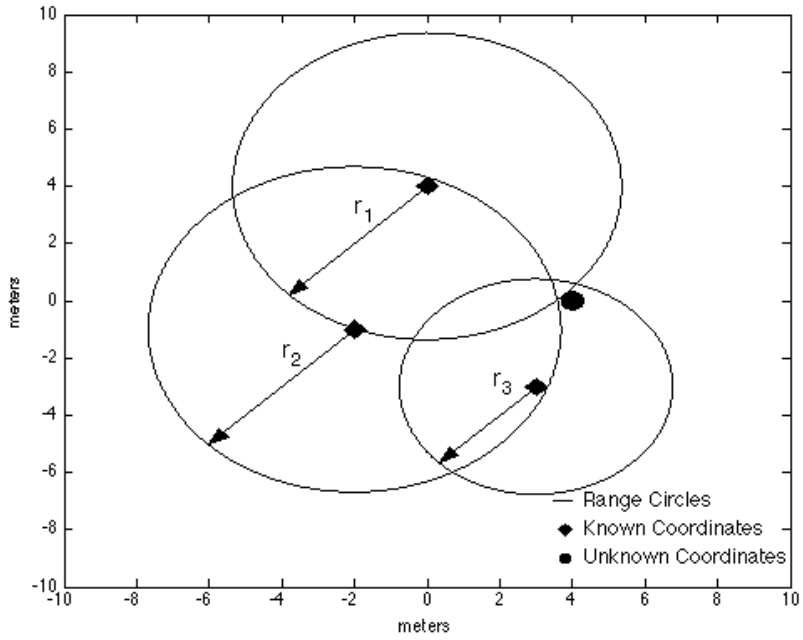

Figure 2.3: Lateration with Erroneous Range Estimates

a non-linear, multi-modal optimization problem that has been solved with a gradient descent solver [28]. More commonly, the problem is defined as the minimization of the squared error between the observed RSS and the predicted RSS as follows:

$$\hat{\boldsymbol{\theta}} = \arg\min_{\boldsymbol{\theta}} \sum_{i=1}^{N} \left(\Omega_i - c + 10\alpha \log_{10}(d_i)\right)^2 \tag{2.9}$$

This formulation of the problem is used extensively in this paper and is referred to as non-linear least squares RSS (NLSR). In Chapter 5, it is shown to be equivalent to the ML estimator if correlated shadowing is assumed to not exist.

Min-max

The min-max algorithm is a simplification of lateration that uses boxes instead of ranging circles [12]. A box is constructed centered at each sensor node with a width and height equivalent to the estimated distance to the emitter, d_i. The two corner coordinates of the box are defined as follows,

$$[x_i - d_i, y_i - d_i],\ [x_i + d_i, y_i + d_i] \tag{2.10}$$

The intersection of the boxes is computed by

$$[\max_i(x_i - d_i), \max_i(y_i - d_i)],\ [\min_i(x_i + d_i), \min_i(y_i + d_i)] \tag{2.11}$$

and the algorithm is completed by averaging the resulting corner coordinates of the box. Min-max is shown to be more robust to errors in the distance estimates than lateration in [12] but is more sensitive to sensor placement. Additionally, depending on the optimization method used to solve RSS lateration, min-max can require significantly fewer operations and will always require the same number of operations to solve.

2.3.2 Range Free

RF Fingerprinting

Radio Frequency (RF) fingerprints are unique spectrum-based characteristics that define a specific location. A fingerprint may consist of a set of RSS measurements, time delays, or a characterization of the multipath for a given location. A combination of these characteristics can also be used; in [8], both TOA and RSS measurements are used to define the fingerprints. Assuming a set of N sensing nodes, M emitter locations can be uniquely defined by M sets of RF fingerprints. This requires an extensive offline measurement campaign to determine the fingerprints at each of the M emitter locations. The emitter must be physically moved to each point and the measurements at each of the sensors must be recorded. Localization is performed by comparing the set of measurements received by the N sensors to the database of fingerprints obtained offline and finding the best match. Techniques for finding the best match include k-nearest neighbor [24], euclidean distance [20], neural networks [19], and bayesian statistics [3].

RF fingerprinting is not a viable option for the proposed problem due to the extensive offline RF mapping required. Also, all sensors must be stationary. If the position of sensor is changed, a new RF mapping must be performed. Additionally, knowledge of the emitter's transmit power and frequency is required and, depending on the fingerprint type, must be a constant.

Centroid

The centroid algorithm estimates the position of an emitter by finding the centroid of the neighboring sensors [2]. The centroid is calculated as the following:

$$\hat{\theta} = \frac{1}{N}\sum_{i=1}^{N}(x_i, y_i) \tag{2.12}$$

where $\hat{\theta}$ is the estimated position of the emitter, N is the number of neighboring sensors, and (x_i, y_i) is the position of sensor i. The algorithm is improved with Weighted Centroid Localization (WCL), which performs a weighted average and assigns weights to the neighboring nodes based on their importance. In [10], weights of either 0.5 or 1 are used based on an RSS threshold that places more importance on sensors that are closer to the emitter. Sensors with an RSS above the threshold receive a weight of 1, and sensors below the threshold receive a weight of 0.5. In [22], rather than use a threshold, the neighboring sensors' are weighted by the inverse of their distance from the emitter as estimated by the log-distance model.

Chapter 3

Review of Differential RSS

3.1 Definition

Differential RSS (DRSS), proposed in [14] and [32], is based on the difference in received power at each of the sensors. The difference operation removes the need to estimate the emitter dependent parameters of frequency, transmit power, and antenna gain. Given the log distance path loss model (Eqn. 7.1), the difference in received power from a single emitter at two sensors k and j is

$$v_{kj} = \Omega_k - \Omega_j \tag{3.1}$$

$$v_{kj} = G_k - G_j + 10\alpha \log_{10}\left(\frac{d_j}{d_k}\right) \tag{3.2}$$

where G_k and G_j are sensor k's and sensor j's antenna gains [13]. If $G_k = G_j$, then these terms can be omitted. This formulation relaxes the number of emitter parameters that need to be estimated, which is advantageous for the proposed problem because only transmit frequency and bandwidth are known parameters. For N sensors, there are $\frac{N(N-1)}{2}$ unique difference pairs. These difference pairs can be separated into $N-1$ independent pairs and $\frac{N(N-1)}{2} - (N-1)$ redundant pairs. Localizing can be performed with either all the pairs or just the independent pairs.

Assuming the log-normal shadowing model and $G_k = G_i, \forall\ k, i$, Eqn. 3.1 becomes

$$v_{kj} = 10\alpha \log_{10}\left(\frac{d_j}{d_k}\right) + X_{ij} \tag{3.3}$$

where X_{ij} is the difference in random shadowing variables X_i and X_j. X_{ij} is Gaussian with zero mean, and the variance is $\sigma_{ij}^2 = 2(1-\rho_{ij})\sigma^2$ [14]. As the correlation coefficient ρ_{ij} increases, the variance of the shadowing variable decreases.

Similar to RSS lateration, the least squares formulation has also been used to solve DRSS localization [14], which is to minimize the squared error of the observations and the model proposed in Eqn. (3.1):

$$\hat{\boldsymbol{\theta}} = \arg\min_{\boldsymbol{\theta}} \sum_{i=1}^{N-1} \sum_{j=i+1}^{N} \left(\Omega_i - \Omega_j - 10\alpha \log_{10} \left(\frac{d_j}{d_i} \right) \right)^2 \tag{3.4}$$

where $\boldsymbol{\theta} = [x, y]$ and N is the number of sensors, and assuming $G_i = G_j \forall i, j$, which will be assumed for the remainder of this paper. Eqn. 3.4 will be referred to as NLSD.

3.2 Geometry

The difference in two ranges results in one distinct circle on which the emitter must lie. Given two sensors k and j located at positions (x_k, y_k) and (x_j, y_j), respectively, and an emitter located at position (x, y), the distances between the emitter and sensors are as follows:

$$d_k^2 = (x - x_k)^2 + (y - y_k)^2 \tag{3.5}$$
$$d_j^2 = (x - x_j)^2 + (y - y_j)^2 \tag{3.6}$$

If the ratio $d_k/d_j = p$ is a constant, then the locus of points (x, y), which satisfy Eqns. 3.5 and 3.6:

$$\begin{aligned}
\left(\frac{d_k}{d_j} \right)^2 &= p^2 \\
d_k^2 &= p^2 d_j^2 \\
(x - x_k)^2 + (y - y_k)^2 &= p^2 (x - x_j)^2 + p^2 (y - y_j)^2 \\
x^2 + 2xx_k + x_k^2 + y^2 + 2yy_k + y_k^2 &= p^2 \left(x^2 + 2xx_j + x_j^2 + y^2 + 2yy_j + y_j^2 \right)
\end{aligned}$$

Grouping like terms and dividing both sides by $(1 - p^2)$ gives the following results:

$$\begin{aligned}
\left[x - \left(\frac{x_k - p^2 x_j}{1 - p^2} \right) \right]^2 + \left[y - \left(\frac{y_k - p^2 y_j}{1 - p^2} \right) \right]^2 &= \\
\left(\frac{x_k - p^2 x_j}{1 - p^2} \right)^2 - \left(\frac{x_k^2 - p^2 x_j^2}{1 - p^2} \right) &+ \\
\left(\frac{y_k - p^2 y_j}{1 - p^2} \right)^2 - \left(\frac{y_k^2 - p^2 y_j^2}{1 - p^2} \right)
\end{aligned}$$

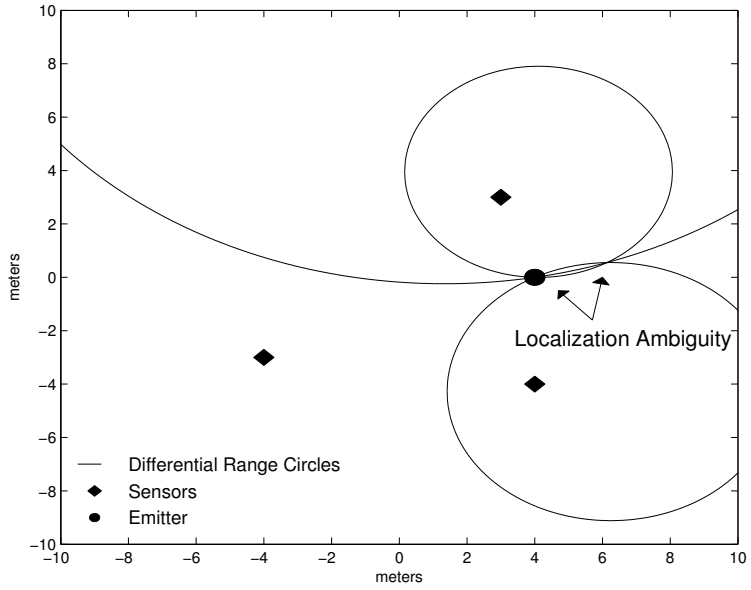

Figure 3.1: DRSS Localization with Three Sensors

This defines a circle in the standard $(x - x_0)^2 + (y - y_0)^2 = r^2$ with the following:

$$\begin{aligned} x_0 &= \frac{x_k - p^2 x_j}{1 - p^2} \\ y_0 &= \frac{y_k - p^2 y_j}{1 - p^2} \\ r^2 &= \left(\frac{x_k - p^2 x_j}{1 - p^2}\right)^2 - \left(\frac{x_k^2 - p^2 x_j^2}{1 - p^2}\right) \\ &+ \left(\frac{y_k - p^2 y_j}{1 - p^2}\right)^2 - \left(\frac{y_k^2 - p^2 y_j^2}{1 - p^2}\right) \end{aligned}$$

From [14], the radius of the difference circle increase as α increases or v_{kj} decreases. It should be noted that a minimum of 4 sensors is required for an unambiguous result. In Fig. 3.1, the 3 differential ranging circles from 3 sensors illustrate an ambiguous result with two intersection points.

3.3 Current State of DRSS

Based on an extensive literature review, work on DRSS appears to be exclusively published in [31], [32], [13], and [14]. These four publications are authored by two separate authors, and

both authors independently present DRSS. Source [31] derives and compares the performance of non-linear least squares (NLS) and linear least squares estimators. Source [14] also derives the NLS estimator and both are identical to Eqn. 3.4. [32] expands on that work and derives the ML estimator and the CRLB for DRSS assuming correlated shadowing does not exist. This work is further detailed in Chapter 5. Source [32] also proves the ML estimator for DRSS (using only independent pairs) and the ML estimator for RSS are equivalent and provide identical solutions. The ML estimator and CRLB will be different in an environment with correlated shadowing. Source [17] does provide the CRLB for DRSS in the presence of correlated shadowing, but only for independent difference pairs.

Source [14] and [13] incorporate spatially correlated shadowing in their simulation results. Using a variant of the NLSD estimator, they show that increasing the correlation coefficient reduces the RMSE of the estimator. The performance is compared to an RSS estimator with perfect knowledge of the close in reference power c. The performance of the DRSS estimator is better than the the performance of the RSS estimator when the correlation coefficient is greater than 0.5.

Chapter 4

Solving NLSD and NLSR

4.1 Method for Simulating RSS Values

The performances of the NLSD and NLSR objective functions given by Eqn. 3.4 and Eqn. 2.9, respectively, are evaluated in a simulated environment. The simulated RSS values are obtained using the models discussed in Chapter 2. The simulated RSS is calculated based on the deterministic model given in Eqn. 7.1, which is solely dependent on the distance from emitter and the PLE. The zero mean, multivariate Gaussian shadowing variable X, is solely defined by its covariance matrix K, defined in Eqn. 7.5. Random samples are generated from this distribution and added to the deterministic RSS values. The covariance matrix K is factorized using Cholesky Factorization to obtain $K = LL^T$. The random samples of the distribution are then $x = Lw$, where $w = [w_1, w_2, ..., w_n]$ is a vector of zero mean, unit variance, and uncorrelated Gaussian random samples. The simulated RSS value Ω_i is then defined mathematically as follows:

$$\Omega_i = c - 10\alpha log_{10}\left(\frac{d_i}{d_0}\right) + x_i \tag{4.1}$$

4.2 Explanation of the Solving Method

The NLSD and NLSR objective functions are non-linear, non-convex, and multi-modal, which makes them difficult to solve with standard optimization techniques. The main focus of this work is to evaluate the respective objective functions rather than the methods for solving them. To this end, the downhill simplex technique is used for all of the non-linear objective functions. Specifically, the Neader-Mead algorithm as implemented in the Matlab function fminsearch is used to solve the objective functions. The specific parameters of the solver are included in Table 4.2. Due to the multi-modal nature of the objective functions,

Table 4.1: Optimization Settings

Parameter	Value
Algorithm	Nelder-Mead simplex direct search
Max Function Evaluations	200 x Number of Variables
Max Iterations	200 x Number of Variables
Function Tolerance	1e-4
Number of Random Starts	10

the performance of the estimator is dependent on the accuracy of the initial estimate. To help ensure the global minima is found, the solvers are initialized with 10 randomly selected estimates. These start positions are uniformly selected from a square box centered on the actual emitter position. If reference power, c, is also being estimated, its start position is uniformly selected from the range $[c-30 : c+30]$. The solver output with the lowest utility value from all of the start positions is selected as the solution. The solution $\hat{\theta} = [\hat{x}, \hat{y}]$ is compared to the actual emitter position $\theta = [x, y]$ and the miss distance or root mean square error (RMSE) is defined as follows:

$$RMSE = \sqrt{(\hat{x} - x)^2 + (\hat{y} - y)^2} \tag{4.2}$$

4.3 Analysis

This section compares the performances of the NLSR and NLSD objective functions. The performance is tested using simulated RSS values based on Eqn. 4.1 and the process outlined in Section 4.2. The average miss distance is determined by averaging the miss distances for 4000 trials. For each trial, a set of sensors and one emitter are randomly positioned in a 1000 x 1000 meter square box. Fig. 4.1 shows the average miss distance for 4 to 16 sensors. The NLSR estimator slightly outperforms the NLSD estimator in all cases, and the difference between the two estimators increases as correlation increases. This difference is a result of the optimization method. If the number of random start positions is increased, the difference between the estimators decreases to zero. On average across all trials, the NLSR estimator takes 197 iterations per start position to find a solution, while the NLSD estimator takes 91 iterations per start position to find a solution. The NLSD estimator takes nearly half the iterations because it is only estimating 2 parameters rather than 3. This difference in iterations is balanced by the fact that it takes the NLSD estimator more initial start positions to find the global solution.

The equivalence of the NLSR and NLSD estimators concurs with [32], which shows their performance is equivalent when correlated shadowing is zero. These results further show that the NLSR and NLSD estimators are equivalent in simulation when correlated shadowing

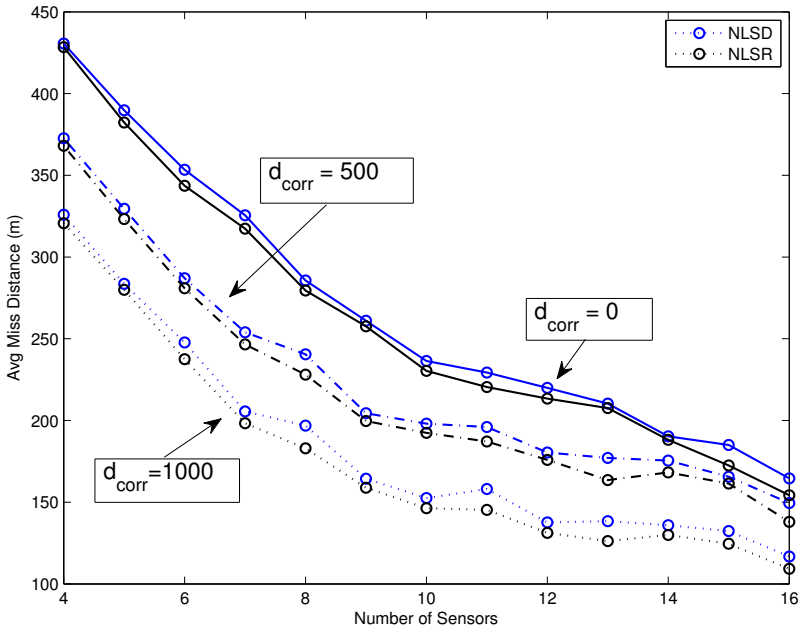

Figure 4.1: Performance Comparison of NLSD and NLSR. $\sigma = 8$, $\alpha = 4$.

is greater than zero. These results also show the average miss distance decreases as the correlation increases. The cause of this relationship is discussed in Section 5.3.1.

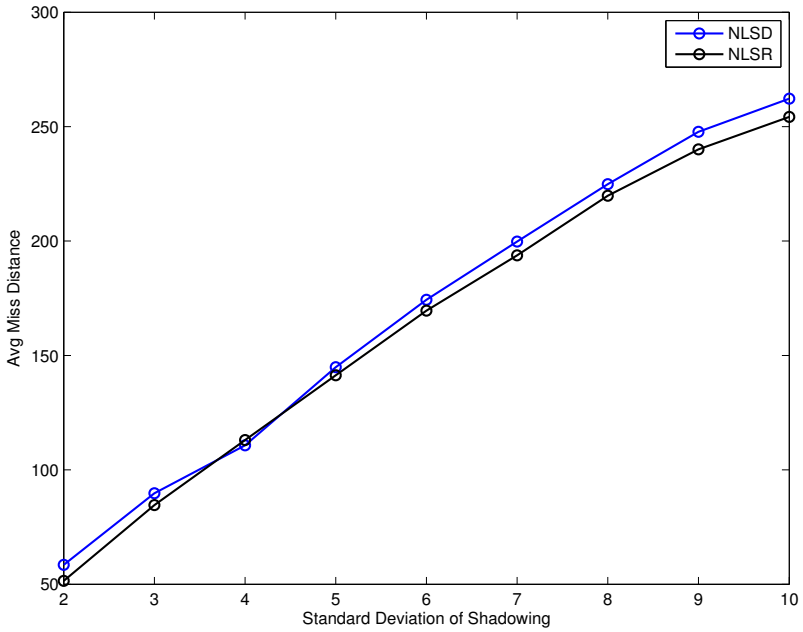

Figure 4.2: Performance Comparison of NLSD and NLSR. $\alpha = 4$, $d_{corr} = 150m$

Chapter 5

Maximum Likelihood Estimator and Cramer Rao Lower Bound

5.1 Maximum Likelihood Estimator

This chapter provides the ML estimators and CRLBs for RSS and DRSS information sources.

5.1.1 ML Estimator Fundamentals

The ML estimator chooses as its solution the parameter that maximizes the probability of the observed data. The likelihood function is the joint probability density function (pdf) of the observed data, and the ML estimator solution is the parameter that maximizes this function. The joint pdf for observed independent and identically distributed (iid) values $x_n = (x_1, x_2, ..., x_n)$ is the following:

$$f(x_1, x_2, ...x_n|\theta) = f(x_1|\theta)f(x_2|\theta)...f(x_n|\theta) \tag{5.1}$$

If the parameter θ is the variable and the observations x_n remain fixed then the likelihood function is as follows:

$$f(\theta|x_1, x_2, ...x_n) = f(\theta|x_1)f(\theta|x_2)...f(\theta|x_n) \tag{5.2}$$

The logarithm of the likelihood function is used more often in practice because it turns the product of terms into a summation:

$$f(\theta|x_1, x_2, ...x_n) = \sum_{i=1}^{n} L(\theta|x_i) \tag{5.3}$$

where $L(\theta|x_i)$ is the logarithm of $f(\theta|x_i)$. Furthermore, the logarithm is monotonic, so maximizing the logarithm of the likelihood function is equivalent to maximizing the likelihood function. The ML estimator is then defined as follows:

$$\hat{\theta} = \arg\max_{\theta} \sum_{i=1}^{n} L(\theta|x_i) \tag{5.4}$$

The pdf for a Gaussian random variable is the following:

$$f(x) = \frac{1}{\sigma\sqrt{2\pi}} e^{-\frac{(x-\mu)^2}{2\sigma^2}} \tag{5.5}$$

5.1.2 Existing ML Estimators

Source [32] derives the ML estimators for RSS and DRSS assuming zero correlation between the shadowing variables X_k and X_j, and the variance is known and unique for each X_k.

ML Estimator for RSS (No Correlation)

From [32], the following vectors are defined:

$$\begin{aligned} \boldsymbol{\theta} &= [x, y, c] \\ \boldsymbol{\Omega} &= [\Omega_1, \Omega_2, ..., \Omega_n] \end{aligned} \tag{5.6}$$

where $\boldsymbol{\Omega}$ is the received power, (x, y) is the emitter's position, and c is the emitter's reference power. Based on Eqn. 5.5, the likelihood function $f(\theta|\Omega)$ is then

$$f(\boldsymbol{\theta}|\boldsymbol{\Omega}) = c_1 \exp\left(-\sum_{i=1}^{n} \frac{\left(\Omega_i - c + 10\alpha \log_{10}(d_i)\right)^2}{2\sigma^2} \right) \tag{5.7}$$

where c_1 is a constant independent of $\boldsymbol{\theta}$. The ML estimator is then the following optimization:

$$\hat{\boldsymbol{\theta}} = \arg\max_{\boldsymbol{\theta}} f(\boldsymbol{\theta}|\boldsymbol{\Omega}) = \arg\min_{\boldsymbol{\theta}} \sum_{i=1}^{n} \frac{\left(\Omega_i - \tilde{\Omega}_i\right)^2}{2\sigma^2} \tag{5.8}$$

where $\tilde{\Omega}_i = c - 10\alpha \log_{10}(d_i)$. This formulation is identical to the NLSR estimator in Eqn. 2.9.

ML Estimator for DRSS (No Correlation)

The information sources for DRSS are the $\frac{n(n-1)}{2}$ unique RSS difference pairs: $\Omega_{kj} = \Omega_k - \Omega_j$, $1 \leq k, j \leq k, j \neq k$. Assuming the correlation, $\rho_{jk} = 0, \forall j, k$, it is not possible to compute

the ML estimator for DRSS directly because the covariance matrix is rank deficient. To simplify, [32] reduces the number of RSS differences to $(n-1)$ and defines fixed integer k in the range $1 < k < n$. The new set of RSS differences, Λ_k is defined as follows:

$$\Lambda_k = [\Omega_{1k}, \Omega_{2k}, ..., \Omega_{(k-1)k}, \Omega_{(k+1)k}, ..., \Omega_{nk}] \tag{5.9}$$

Based on Λ_k, the following ML estimator for $\boldsymbol{\theta} = [x, y]$ can be derived with the proof shown in [32],

$$\hat{\boldsymbol{\theta}} = \arg\min_{\boldsymbol{\theta}} \sum_{i=1}^{n} \sigma_i^{-2} (\overline{\Omega} - 10\alpha\overline{\log_{10}(d)} - \overline{c})^2 \tag{5.10}$$

where the following averages are defined as the following:

$$\begin{aligned} \overline{\Omega} &= \sum_{i=1}^{n} \frac{\sum_{j=1}^{n} \sigma_j^2}{\sigma_i^{-2}} \Omega_i \\ \overline{\log_{10}(d)} &= \sum_{i=1}^{n} \frac{\sum_{j=1}^{n} \sigma_j^2}{\sigma_i^{-2}} \log_{10}(d_i) \\ \overline{c} &= \overline{\Omega} + 10\alpha\overline{\log_{10}(d_i)} \end{aligned} \tag{5.11}$$

Source [32] further shows this ML estimator for $[x, y]$ is equivalent to the ML estimator based on RSS information shown in Eqn. 5.8.

5.1.3 New Proposed ML Estimators

The ML estimators derived in [32] assume the random shadowing variables are not correlated. The results in Chapter 7 show the correlation between two shadowing variables is dependent on the distance between them. It is necessary to derive ML estimators for RSS and DRSS information sources in the presence of spatially correlated shadowing.

ML Estimator for RSS (With Correlation)

The pdf for a multivariate Gaussian random variable is as follows:

$$f(x_1, x_2, ..., x_n) = \frac{1}{(2\pi)^{k/2} |\boldsymbol{\Gamma}|^{1/2}} \exp\left(-\frac{1}{2} (\boldsymbol{x} - \boldsymbol{\mu})^T \boldsymbol{\Gamma}^{-1} (\boldsymbol{x} - \boldsymbol{\mu}) \right) \tag{5.12}$$

where $\boldsymbol{\Gamma}$ is the covariance matrix and $\boldsymbol{\mu}$ is the mean vector. The likelihood function for RSS assuming the log-distance model with correlated random variables is as follows:

$$f(\boldsymbol{\theta}|\boldsymbol{\Omega}) = c_1 \exp\left((\boldsymbol{\Omega} - \tilde{\boldsymbol{\Omega}})^T \boldsymbol{\Gamma}^{-1} (\boldsymbol{\Omega} - \tilde{\boldsymbol{\Omega}}) \right) \tag{5.13}$$

where c_1 is a constant independent of $\boldsymbol{\theta}$, $\boldsymbol{\theta} = [x, y, c]$, $\boldsymbol{\Omega} = [\Omega_1, \Omega_2, ..., \Omega_n]$, $\tilde{\boldsymbol{\Omega}} = [\tilde{\Omega}_1, \tilde{\Omega}_2, ..., \tilde{\Omega}_n]$, and the covariance matrix $\boldsymbol{\Gamma}$ is as follows:

$$\begin{aligned} \Gamma_{jk} &= \rho_{jk}\sigma^2, j \neq k \\ \Gamma_{jk} &= \sigma^2, j = k \end{aligned} \tag{5.14}$$

Since σ is assumed to be the same for all Ω, $\boldsymbol{\Gamma}$ simply becomes the following:

$$\begin{aligned} \Gamma_{jk} &= \rho_{jk}, j \neq k \\ \Gamma_{jk} &= 1, j = k \end{aligned} \tag{5.15}$$

The ML estimator is then the following:

$$\hat{\boldsymbol{\theta}} = \arg\min_{\boldsymbol{\theta}} \left((\boldsymbol{\Omega} - \tilde{\boldsymbol{\Omega}})^T \boldsymbol{\Gamma}^{-1} (\boldsymbol{\Omega} - \tilde{\boldsymbol{\Omega}}) \right) \tag{5.16}$$

ML Estimator for DRSS (With Correlation)

The ML estimator for position based on DRSS in the presence of correlated shadowing is rank deficient similar to the case with no correlated shadowing. This section provides the ML estimator although it cannot be solved due to the rank deficient covariance matrix. It is assumed that all shadowing variables X_j have the same variance, σ^2. And the correlation between X_j and X_k is ρ_{jk} and is a known value. Let $\boldsymbol{\theta}$ be redefined as $\boldsymbol{\theta} = [x, y]$. The likelihood function is then

$$f(\theta|\Omega_{jk}) = c_1 \exp\left((\Omega_{jk} - \tilde{\Omega}_{jk})^T \boldsymbol{\Gamma}^{-1} (\Omega_{jk} - \tilde{\Omega}_{jk}) \right) \tag{5.17}$$

where $\tilde{\Omega}_{jk} = 10\alpha \log_{10}(\frac{d_k}{d_j})$. The derivation of the covariance matrix, $\boldsymbol{\Gamma}$ follows:

$$\begin{aligned} COV(\Omega_{jk}, \Omega_{gh}) &= E[X_{jk} X_{gh}] \\ &= E\left[(X_j - X_k)(X_g - X_h) \right] \\ = E[X_j X_g] - E[X_j X_h] - E[X_k X_g] + E[X_k X_h] \\ &= (\rho_{jg} - \rho_{jh} - \rho_{kg} + \rho_{kh})\sigma^2 \end{aligned} \tag{5.18}$$

and similarly,

$$\begin{aligned} COV(\Omega_{jk}, \Omega_{jh}) &= E\left[(X_j - X_k)(X_j - X_h) \right] \\ = E[X_j^2] - E[X_j X_h] - E[X_k X_j] + E[X_k X_h] \\ &= \sigma^2 + (-\rho_{jh} - \rho_{kj} + \rho_{kh})\sigma^2 \end{aligned} \tag{5.19}$$

and lastly,

$$COV(\Omega_{jk}, \Omega_{jk}) = VAR(\Omega_{jk}) = 2(1 - \rho_{jk})\sigma^2 \tag{5.20}$$

With the elements of $\mathbf{\Gamma}$ defined by Eqns. 5.18, 5.19, and 5.20, the ML estimator is then the following:

$$f(\theta|\Omega) = \arg\min_{\theta} \left((\Omega_{jk} - \tilde{\Omega}_{jk})^T \mathbf{\Gamma}^{-1} (\Omega_{jk} - \tilde{\Omega}_{jk}) \right), \forall 1 \leq k, j \leq k, j \neq k \tag{5.21}$$

And if σ is a constant, then the elements of $\mathbf{\Gamma}$ can be simplified to the following:

$$\Gamma(\Omega_{jk}, \Omega_{gh}) = (\rho_{jg} - \rho_{jh} - \rho_{kg} + \rho_{kh}) \tag{5.22}$$

$$\Gamma(\Omega_{jk}, \Omega_{jh}) = 1 + (-\rho_{jh} - \rho_{kj} + \rho_{kh}) \tag{5.23}$$

$$\Gamma(\Omega_{jk}, \Omega_{jk}) = 2(1 - \rho_{jk}) \tag{5.24}$$

5.2 Cramér Rao Lower Bound

This section provides the CRLBs for RSS information and DRSS information sources in the presence of correlated shadowing.

5.2.1 CRLB Fundamentals

The CRLB on the covariance of any unbiased estimator is given by

$$E[(\hat{\boldsymbol{\theta}} - \boldsymbol{\theta})(\hat{\boldsymbol{\theta}} - \boldsymbol{\theta})^T] \geq J^{-1} \tag{5.25}$$

where J is the Fisher information matrix (FIM) [9]. Let $\mu(\theta) = [\mu_1(\theta), \mu_2(\theta), ..., \mu_n(\theta)$ and $\mathbf{\Gamma}$ be the covariance matrix of a multivariate normal distribution, then the elements of the FIM are defined as follows:

$$J_{m,n} = \frac{\partial \boldsymbol{\mu}^T}{\partial \theta_m} \mathbf{\Gamma}^{-1} \frac{\partial \boldsymbol{\mu}}{\partial \theta_n} + \frac{1}{2} tr \left(\mathbf{\Gamma}^{-1} \frac{\partial \mathbf{\Gamma}}{\partial \theta_m} \mathbf{\Gamma}^{-1} \frac{\partial \mathbf{\Gamma}}{\partial \theta_n} \right) \tag{5.26}$$

where T is the transpose and tr is the trace of the matrix. And in the case where $\mathbf{\Gamma}$ is not dependent on θ, the the FIM is the following:

$$J_{m,n} = \frac{\partial \boldsymbol{\mu}^T}{\partial \theta_m} \mathbf{\Gamma}^{-1} \frac{\partial \boldsymbol{\mu}}{\partial \theta_n} \tag{5.27}$$

Let the true location of the emitter be $\boldsymbol{\theta} = [x, y]$. If position error is defined as $e = ||\hat{\boldsymbol{\theta}} - \boldsymbol{\theta}||$, the root mean square error (RMSE) is then $\sqrt{E[e^2]}$ and the lower bound on the RMSE, or average miss distance is the following:

$$\begin{aligned} \sqrt{E[e^2]} &= \sqrt{E(\hat{x} - x)^2 + E(\hat{y} - y)^2} \\ &\geq \sqrt{[J^{-1}]_{1,1} + [J^{-1}]_{2,2}} \end{aligned} \tag{5.28}$$

5.2.2 Existing CRLB

RSS (Without Correlation)

The CRLB for RSS localization without correlation in [18]. The FIM, J, is defined as follows:

$$\begin{aligned} J_{1,1} &= \frac{1}{\sigma^2}\sum_{i=1}^{N}\left(\frac{\partial f(\boldsymbol{\theta})^T}{\partial x}\right)^2 \\ J_{2,2} &= \frac{1}{\sigma^2}\sum_{i=1}^{N}\left(\frac{\partial f(\boldsymbol{\theta})^T}{\partial y}\right)^2 \\ J_{2,3} = J_{3,2} &= \frac{1}{\sigma^2}\sum_{i=1}^{N}\frac{\partial f(\boldsymbol{\theta})^T}{\partial x}\frac{\partial f(\boldsymbol{\theta})}{\partial y} \end{aligned} \tag{5.29}$$

where

$$\begin{aligned} f_i(\boldsymbol{\theta}) &= 10\alpha\log_{10}(d_i) \\ \frac{\partial f_i(\boldsymbol{\theta})}{\partial x} &= -\frac{10\alpha}{\ln 10}\frac{x-x_i}{d_i^2} \\ \frac{\partial f_i(\boldsymbol{\theta})}{\partial y} &= -\frac{10\alpha}{\ln 10}\frac{y-y_i}{d_i^2} \end{aligned} \tag{5.30}$$

The lower bound of the average miss distance is then defined as follows:

$$\sqrt{E[e^2]} \geq \sqrt{[J^{-1}]_{1,1} + [J^{-1}]_{2,2}} \tag{5.31}$$

In this derivation, the reference power c is assumed to be known. The CRLB for RSS localization with unknown reference power, c, has recently been published in [29].

DRSS (Without Correlation)

The CRLB for DRSS without correlation is derived in [32]. The difference pairs are defined by Eqn. 5.9 and only include the n independent pairs. The CRLB cannot be directly determined for the entire set of difference pairs because the covariance matrix is rank deficient. The lower bound on the average miss distance is defined as follows:

$$\sqrt{E[e^2]} \geq \frac{ln(10)}{10\alpha}\left[\sum_{i=1}^{n}\sigma_i^{-2}\right]^{-\frac{1}{2}}\sqrt{\frac{\overline{\tau^2}-(\overline{\tau})^2+\overline{q^2}-(\overline{q})^2}{det\begin{bmatrix}\overline{\tau^2}-(\overline{\tau})^2 & \overline{\tau q}-\overline{\tau q}\\ \overline{\tau q}-\overline{\tau q} & \overline{q^2}-(\overline{q})^2\end{bmatrix}}} \tag{5.32}$$

where

$$\tau_i = \frac{x-x_i}{d_i^2}, \quad q = \tfrac{y-y_i}{d_i^2} \tag{5.33}$$

and averages of τ and q are defined as follows:

$$\overline{\tau} = \sum_{i=1}^{n} w_i \tau_i, \quad \overline{q} = \textstyle\sum_{i=1}^{n} w_i q_i \tag{5.34}$$

$$\overline{\tau^2} = \sum_{i=1}^{n} w_i \tau_i^2, \quad \overline{q^2} = \textstyle\sum_{i=1}^{n} w_i q_i^2 \tag{5.35}$$

$$\overline{\tau q} = \sum_{i=1}^{n} w_i \tau q \tag{5.36}$$

and $w_i = \frac{\sum_{j=1}^{n} \sigma_j^2}{\sigma_i^2}$. The proof is omitted here, but [32] shows the CRLB for DRSS in Eqn. 5.32 is equivalent to the CRLB for RSS in Eqn. 5.31.

5.2.3 New Proposed CRLB

RSS (With Correlation)

Source [17] derives the CRLB for RSS localization in the presence of correlated shadowing, but the reference power is known, and the correlation is constant for all sensors. This section presents the CRLB for RSS localization with correlated shadowing (based on Eqn. 2.6) and with unknown reference power c. The FIM, J, for n RSS observations in the presence of correlated shadowing where $X \sim N(\mu(\theta), \mathbf{\Gamma})$ and $\boldsymbol{\theta} = [x, y, c]$ is defined as the following:

$$\begin{aligned}
J_{1,1} &= \frac{\partial f(\boldsymbol{\theta})^T}{\partial x} \mathbf{\Gamma}^{-1} \frac{\partial f(\boldsymbol{\theta})}{\partial x} \\
J_{2,2} &= \frac{\partial f(\boldsymbol{\theta})^T}{\partial y} \mathbf{\Gamma}^{-1} \frac{\partial f(\boldsymbol{\theta})}{\partial y} \\
J_{3,3} &= \frac{\partial f(\boldsymbol{\theta})^T}{\partial c} \mathbf{\Gamma}^{-1} \frac{\partial f(\boldsymbol{\theta})}{\partial c} \\
J_{1,2} = J_{2,1} &= \frac{\partial f(\boldsymbol{\theta})^T}{\partial x} \mathbf{\Gamma}^{-1} \frac{\partial f(\boldsymbol{\theta})}{\partial y} \\
J_{2,3} = J_{3,2} &= \frac{\partial f(\boldsymbol{\theta})^T}{\partial c} \mathbf{\Gamma}^{-1} \frac{\partial f(\boldsymbol{\theta})}{\partial y} \\
J_{1,3} = J_{3,1} &= \frac{\partial f(\boldsymbol{\theta})^T}{\partial c} \mathbf{\Gamma}^{-1} \frac{\partial f(\boldsymbol{\theta})}{\partial x}
\end{aligned} \tag{5.37}$$

where $\frac{\partial f(\boldsymbol{\theta})^T}{\partial x} = [\frac{\partial f_1(\boldsymbol{\theta})}{\partial x}, \frac{\partial f_2(\boldsymbol{\theta})}{\partial x}, ..., \frac{\partial f_n(\boldsymbol{\theta})}{\partial x}]$, $\boldsymbol{\Gamma}$ is defined by Eqn. 7.5, and

$$\begin{aligned} f_i(\boldsymbol{\theta}) &= c - 10\alpha \log_{10}(d_i) \\ \frac{\partial f_i(\boldsymbol{\theta})}{\partial x} &= -\frac{10\alpha}{\ln 10}\frac{x - x_i}{d_i^2} \\ \frac{\partial f_i(\boldsymbol{\theta})}{\partial y} &= -\frac{10\alpha}{\ln 10}\frac{y - y_i}{d_i^2} \\ \frac{\partial f_i(\boldsymbol{\theta})}{\partial c} &= 1 \end{aligned} \tag{5.38}$$

where $[x_i, y_i]$ is the position of sensor i. The lower bound for the average miss distance is then the following:

$$\sqrt{E[e^2]} \geq \sqrt{[J^{-1}]_{1,1} + [J^{-1}]_{2,2}} \tag{5.39}$$

DRSS (With Correlation)

The FIM for DRSS-based observations in the presence of correlated shadowing where $X \sim N(\mu(\theta), \boldsymbol{\Gamma})$ is defined as

$$\begin{aligned} J_{1,1} &= \frac{\partial f(\boldsymbol{\theta})^T}{\partial x}\boldsymbol{\Gamma}^{-1}\frac{\partial f(\boldsymbol{\theta})}{\partial x} \\ J_{2,2} &= \frac{\partial f(\boldsymbol{\theta})^T}{\partial y}\boldsymbol{\Gamma}^{-1}\frac{\partial f(\boldsymbol{\theta})}{\partial y} \\ J_{1,2} = J_{2,1} &= \frac{\partial f(\boldsymbol{\theta})^T}{\partial x}\boldsymbol{\Gamma}^{-1}\frac{\partial f(\boldsymbol{\theta})}{\partial y} \end{aligned} \tag{5.40}$$

where $\frac{\partial f(\boldsymbol{\theta})^T}{\partial x} = [\frac{\partial f_1(\boldsymbol{\theta})}{\partial x}, \frac{\partial f_2(\boldsymbol{\theta})}{\partial x}, ..., \frac{\partial f_m(\boldsymbol{\theta})}{\partial x}]$, $m = \frac{n(n-1)}{2}$ is the number of DRSS observations, and $\boldsymbol{\Gamma}$ is the defined by Eqns. 5.22, 5.23, and 5.24. In this case $f_i(\boldsymbol{\theta})$ is defined as follows:

$$\begin{aligned} f_i(\boldsymbol{\theta}) &= 10\alpha \log_{10}\left(\frac{||\boldsymbol{\theta} - \boldsymbol{\theta}_k||}{||\boldsymbol{\theta} - \boldsymbol{\theta}_j||}\right) \\ &= 10\alpha \log_{10}(||\boldsymbol{\theta} - \boldsymbol{\theta}_{kj}||) \end{aligned} \tag{5.41}$$

where $\boldsymbol{\theta}_{kj} = [x_{kj}, y_{kj}] = [\frac{x_k - p^2 x_j}{1-p^2}, \frac{y_k - p^2 y_j}{1-p^2}]$ and $p = \frac{d_k}{d_j}$. For more details see Section 3.2. The partial derivatives of $f_i(\boldsymbol{\theta})$ are as follows:

$$\begin{aligned} \frac{\partial f_i(\boldsymbol{\theta})}{\partial x} &= \frac{10\alpha}{\ln 10}\frac{x - x_i}{||\boldsymbol{\theta} - \boldsymbol{\theta}_i||^2} \\ \frac{\partial f_i(\boldsymbol{\theta})}{\partial y} &= \frac{10\alpha}{\ln 10}\frac{y - y_i}{||\boldsymbol{\theta} - \boldsymbol{\theta}_i||^2} \end{aligned} \tag{5.42}$$

The lower bound on the average miss distance is then the following:

$$\sqrt{E[e^2]} \geq \sqrt{[J^{-1}]_{1,1} + [J^{-1}]_{2,2}} \tag{5.43}$$

Since $\mathbf{\Gamma}$ is rank deficient, it is not possible to directly solve the CRLB for position location based on all DRSS information pairs. The CRLB can be solved using pseudo-inverse methods, but because of the singular nature of the $\mathbf{\Gamma}$, the results are not valid. In [17], the CRLB for independent DRSS pairs in the presence of correlated shadowing is given, and it is proven the CRLBs for RSS (with perfect knowledge of reference power) and DRSS (based on independent pairs) in the presence of correlated shadowing are as follows:

$$\sqrt{E[e_{RSS}^2]} \leq \sqrt{E[e_{DRSS}^2]} \tag{5.44}$$

As stated earlier, the CRLBs for RSS (with no knowledge of reference power) and DRSS (based on independent pairs) without correlated shadowing are equivalent. Based on this, and the fact that DRSS is solely based on RSS information sources, it can be inferred that the CRLB for RSS (with no knowledge of reference power) in the presence of correlated shadowing is also a valid bound for DRSS.

5.3 Analysis of ML Estimator and CRLB

This section provides analysis of the ML estimator and the CRLB for RSS information sources; specifically, the ML estimator in Eqn. 5.21, referred to as MLER, and the lower bound on average miss distance specified in Eqn. 5.43, referred to as CRLB. The MLER is tested using simulated RSS values based on Eqn. 4.1. The parameters for the simulated RSS values are specified for each test. The emitter and sensors are randomly positioned in a 1000-by-1000 meter box for each trial, and the results from 3000 trials are averaged to determine the average miss distance. The error for a position estimate from trial k is defined as follows:

$$e_k = ||\boldsymbol{\theta}_k - \hat{\boldsymbol{\theta}}_k||$$

where $\boldsymbol{\theta}_k = [x, y]$ is the emitter's actual position and $\hat{\boldsymbol{\theta}}_k = [\hat{x}, \hat{y}]$ is the emitter's estimated position. The location errors from a set of n tests with independent shadowing realizations and a fixed geometry classified as t is defined as $\boldsymbol{e}^{(t)} = [e_1, e_2, ..., e_n]$. The lower bound on the RMSE is as follows:

$$\sqrt{E(\boldsymbol{e}^{(t)^2})} \geq CRLB^{(t)}$$

where $CRLB^{(t)}$ is the CRLB for the fixed geometry classified as t. Based on this, then the following is true:

$$\frac{1}{M}\sum_{i=1}^{M}\sqrt{E(\boldsymbol{e}^{(i)^2})} \geq \frac{1}{M}\sum_{i=1}^{M} CRLB^{(i)} \tag{5.45}$$

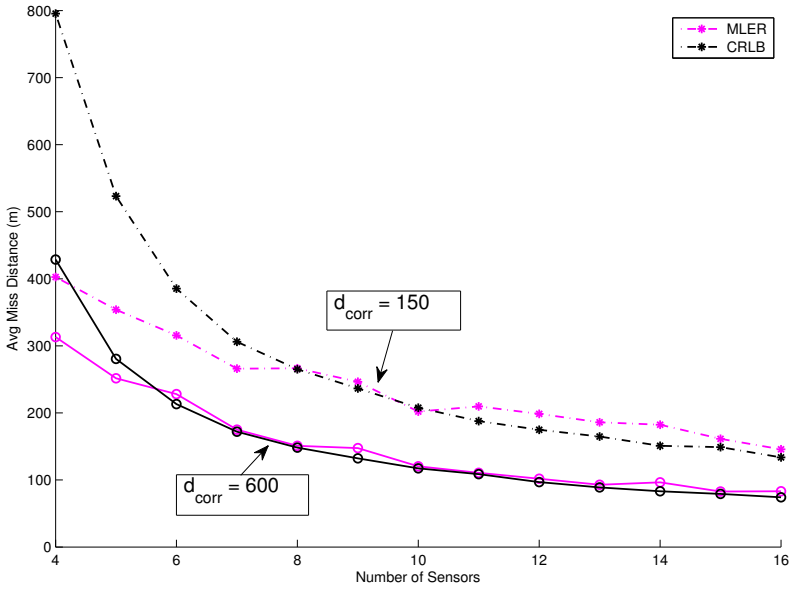

Figure 5.1: Performance of MLER Compared to CRLB. $\sigma = 8$, $\alpha = 4$

In this paper, $n = 1$ and $M = 3000$. In Fig. 5.1, the MLER is compared to the CRLB for 4 to 16 sensors when $\alpha = 4$, $\sigma = 8dB$, and d_{corr} is 150 and 600 meters. The MLER closely matches the bound provided by the CRLB when the number of sensors is high. The CRLB is not a valid bound when the number of sensors is small because the MLER achieves a lower average miss distance. These results concur with [18] and [21], which show that similar ML estimators are biased and increasingly biased as the number of sensors decreases. The CRLB in this paper is the bound for an unbiased estimator so it is expected that it is not valid when the number of sensors is low. The bias can also be attributed to the fact that only one shadowing realization per geometry is used ($n = 1$). A different result may be expected when the number of shadowing realizations n is increased. Fig. 5.2 shows the CRLB and MLER versus σ. This case illustrates the MLER is also biased when σ is high (above 6) because it outperforms the CRLB. So the CRLB is only a valid bound on the MLER when the shadowing variance is low and the number of sensors is high. The MLER is only guaranteed to be the optimal estimator when the number of sensors tends to infinity [15]. It should also be noted that the MLER is less biased as correlation increases.

5.3.1 The Effect of Correlation, Variance, and α on the CRLB

This section provides numerical analysis of the effect of correlation, variance, and α on the CRLB. The tests are conducted by randomly positioning sensors and an emitter in a 1000-by-1000 meter square for 3000 independent trials. The CRLB for each trial is calculated and

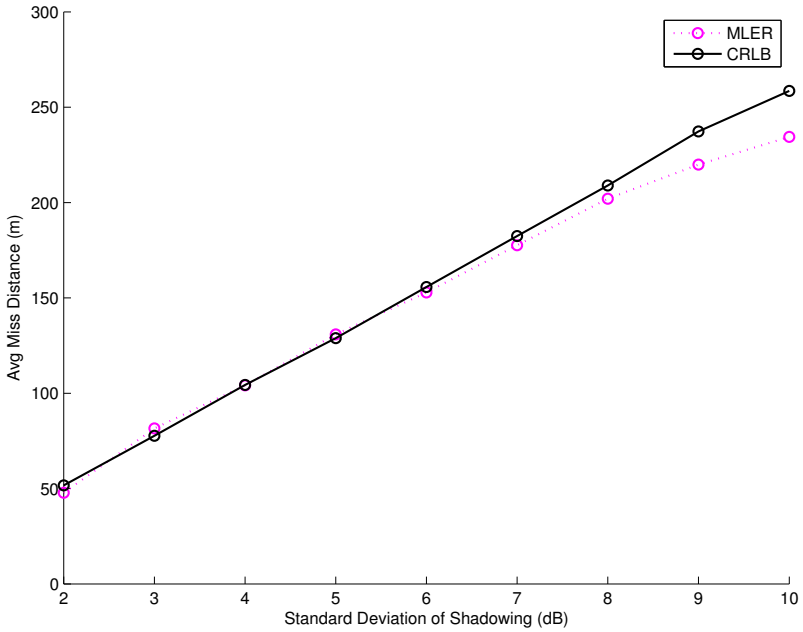

Figure 5.2: Performance of MLER Compared to CRLB. $\alpha = 4$, $d_{corr} = 150m$, 10 sensors

the average across all trials is denoted as the average miss distance.

The Effect of Correlation on the CRLB

Similar to the simulation results in the Chapter 4, Fig. 5.3 and Fig. 5.4 show that as correlated shadowing increases, the CRLB decreases. In Fig. 5.3, the correlation is based on Eqn. 2.6 and in Fig. 5.4, the correlation is a constant value. This result is contrary to what one's intuition might suggest about correlated shadowing. The relationship can be explained by analyzing the formulation of the NLSD estimator. In this estimator, the variance of each residual is assumed to be $\sigma^2 = 2(1-\rho)\sigma_x^2$ where σ_x^2 is the shadowing variance for each of the links between the emitter and the sensors. Here it is evident that as ρ increases, the variance of the residuals decreases and thus will result in a better position estimate. The effect of correlation can also be explained by analyzing the FIM (which is inversely proportional to CRLB). The first element of the FIM defined by 5.37 is as follows:

$$J_{1,1} = \frac{\frac{1}{N}F_1(1-\rho) + \rho N^2(F_1 - F_2)}{\sigma^2\left(-(N-1)\rho^2 + (N-2)\rho + 1\right)} \tag{5.46}$$

where N is the number of sensors, σ^2 is the shadowing variance, $\rho = \rho_{ij} \forall\ i, j$ is the constant correlation, and

$$F_1 \triangleq \frac{1}{N} \sum_{i=1}^{N} f_i'(\boldsymbol{\theta})^2,\ F_2 \triangleq \left(\frac{1}{N} \sum_{i=1}^{N} f_i'(\boldsymbol{\theta}) \right)^2 \tag{5.47}$$

where $f_i'(\boldsymbol{\theta})$ is defined by Eqn. 5.38. As the number of sensors N tends to infinity,

$$J_{1,1} \to \frac{N(F_1 - F_2)}{\sigma^2(1-\rho)} \tag{5.48}$$

From this formulation, it is evident that the FIM increases with N and ρ and decreases with σ as long as $F_1 - F_2 \geq 0$. Based on the Cauchy-Schwartz inequality, this would only occur if $f_i(\boldsymbol{\theta})$ was independent of the index i as shown in [11]. Therefore, the FIM increases for $[x, y]$ with correlation, but decreases for $[c]$ with correlation. The overall result is an increase in the FIM as correlation increases.

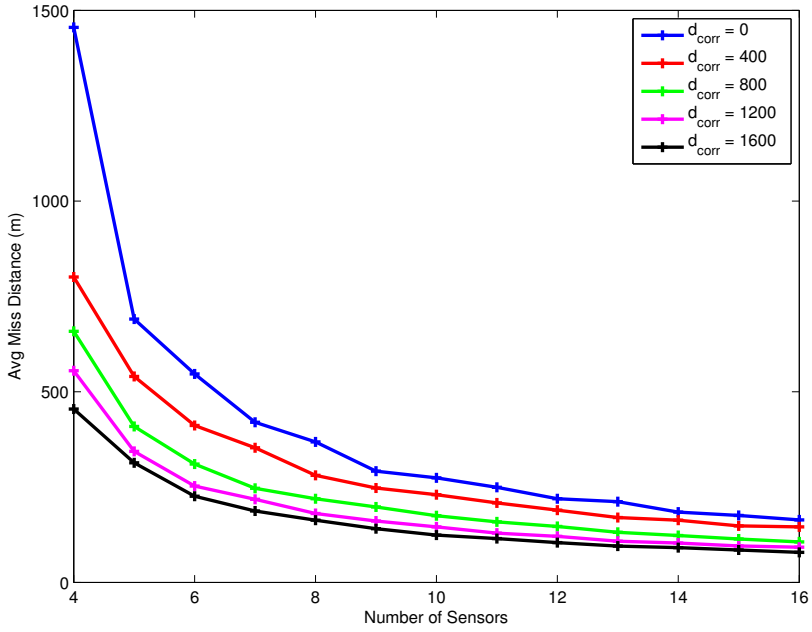

Figure 5.3: CRLB with Correlation Based on Eqn. 2.6

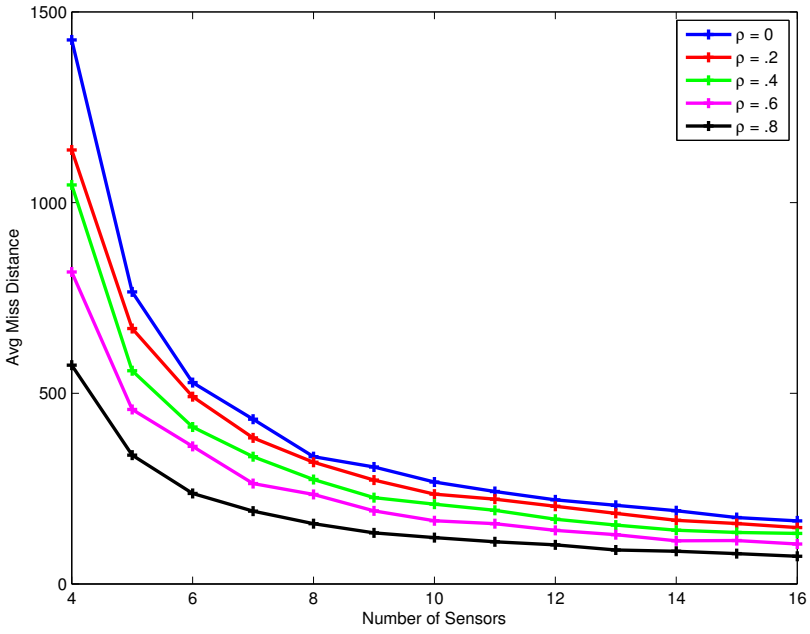

Figure 5.4: CRLB with Constant Correlation for all Sensors

The Effect of Variance on the CRLB

Fig. 5.5 shows that variance has a proportional relationship with the CRLB. This result concurs with simulation results shown in Fig. 4.2.

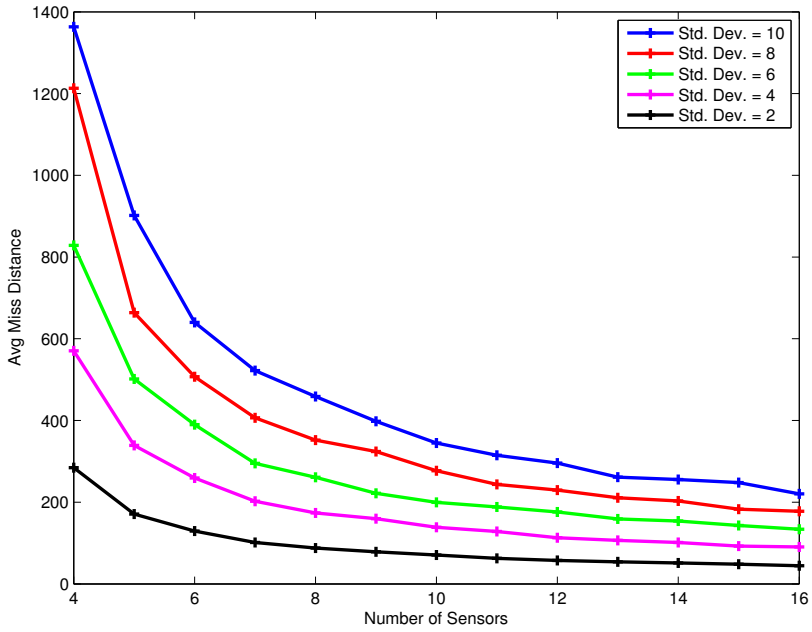

Figure 5.5: CRLB with Varying σ

The Effect of α on the CRLB

Fig. 5.6 shows that α has an inversely proportional relationship with the CRLB. This result concurs with other work in [14].

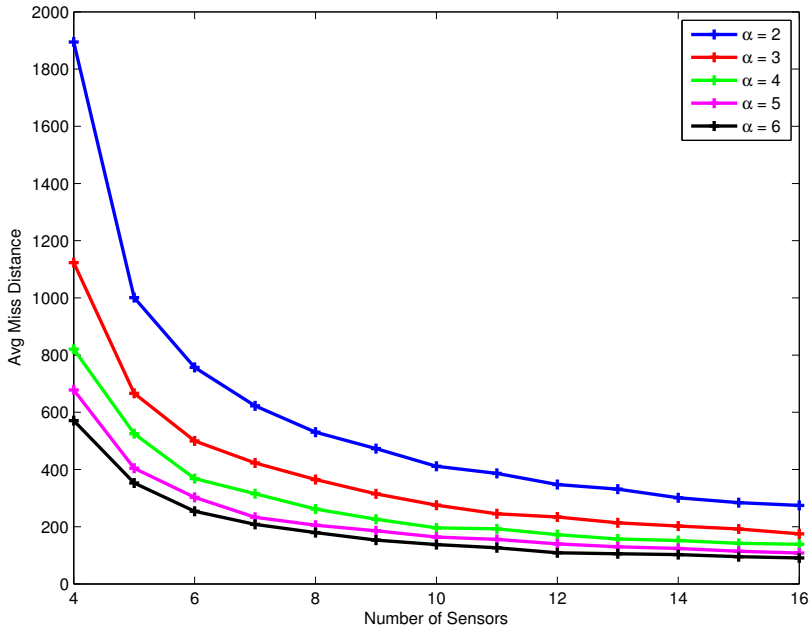

Figure 5.6: CRLB with Varying α

5.4 Geometric Dilution of Precision

Geometric dilution of precision (GDOP) is primarily used in the context of the GPS where it describes the position errors that can be attributed to the location of the satellites. GDOP can be applied to any positioning system and it describes the effect the geometry of the elements of the system has on the error of the estimated position. It relates how changes in the measurements will affect the position estimate. Specifically, GDOP translates range or measurement domain errors to position errors. For most range based systems, the ideal configuration that results in the lowest GDOP is the one with the largest volume created by the sensors (or emitters in the case of GPS). This configuration is when the sensors are equally spaced on a circle with the emitter at the center of the circle. A GDOP term can be derived for RSS-based positioning in the presence of correlated shadowing by removing all variables from the CRLB that do not relate to the geometry. In this case, the CRLB in Eqn. 5.43 is evaluated with α and σ^2 removed. This new formulation is then solely defined by d_{corr} and the positions of the emitter and the sensors. It should be noted α has a direct inversely proportional relationship with the CRLB and σ has a directly proportional relationship with the CRLB. The GDOP formulation makes it is possible to determine the optimal geometric configurations for RSS-based positioning for specific values of d_{corr}.

5.4.1 Sensor Geometry

In this section, the effect of sensor and emitter geometry on the CRLB is evaluated. This GDOP formulation will be referred to as g and is a metric of expected localization performance based on the sensor geometry. It is defined as

$$g = CRLB_{unit} \tag{5.49}$$

where $CRLB_{unit}$ is the CRLB evaluated when $\alpha = 1$ and $\sigma = 1$. Fig. 5.7 shows the distribution of g for three different general sensor configurations described in Table 5.1. For this test, the box size is 2000-by-2000 meters, the number of sensors is 8, and $d_{corr} = 150m$. The results from 10,000 independent trials are included in each of the distributions. From these distributions, it is clear that the geometry of the sensors and emitter has a significant effect on the lower bound of the average miss distance. Fig. 5.8 shows the mean value of each distribution for varying d_{corr} values. The best configuration for all values of d_{corr} ranging from 100 to 1000 meters is Configuration 2. When correlation is low, Configuration 3 outperforms Configuration 1, but as correlation increases Configuration 1 outperforms Configuration 3.

Table 5.1: Sensor Configurations

Configuration 1	Emitter is centered and the sensors are confined to the lower left quadrant of the box.
Configuration 2	Emitter is centered in the box and the sensors are randomly placed in the box.
Configuration 3	Emitter and sensors are randomly placed in the box.

5.4.2 Visualizing the Effect of Correlation

This section reviews the effect of correlated shadowing on GDOP for fixed geometric sensor configurations. It has already been shown that an increase in correlation will decrease the CRLB (and consequently g). This section analyzes how g changes for a fixed sensor configuration when the correlation is changed. Fig. 5.9 and Fig. 5.10 show the surface of g^{-1} for two different fixed sensor configurations. The black lines represent the sensor locations. The surface is generated by calculating g at each point on a square grid centered at [0,0]. The grid is 1200 x 1200 meters on the sides and has a grid spacing of 20. Each grid point represents a value of g for an emitter located at that respective point. From Fig. 5.9 and Fig. 5.10, it is evident that the surface of g^{-1} is significantly different when the sensors are in a circle versus when the sensors are in a line. Viewing the surface of g^{-1} in this manner gives insight into the optimal performance areas for a given sensor configuration.

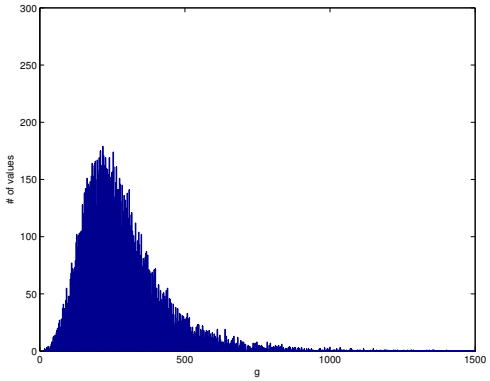

(a) Configuration 1: Emitter is centered and the sensors are confined to the lower left quadrant of the box.

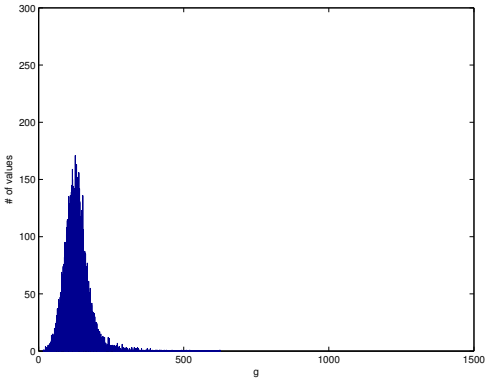

(b) Configuration 2: Emitter is centered in the box and the sensors are randomly placed in the box.

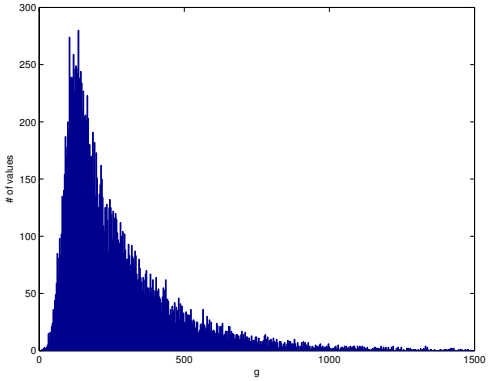

(c) Configuration 3: Emitter and sensors are randomly placed in the box.

Figure 5.7: Distributions of g

For instance, the optimal location for the emitter to be located with the circle configuration is within the circle but not necessarily at the center of the circle. The optimal location for the emitter to be located with the line configuration is along a line close to and parallel to the line of sensors.

A series of three experiments are conducted that illustrate the effect of correlated shadowing on the optimal sensor geometry. For the first experiment, eight sensors are equally spaced on the circumference of a circle centered at [0,0] with a radius of 500 meters as shown in Fig. 5.9. One metric of interest is the mean value of g across the entire 1200-by-1200 meter grid surface. This metric gives an indication of the average position error to be expected within the 1200-by-1200 meter area for the given fixed sensor configuration. To find this value, all values of g on the grid are averaged with the exception of those that lie on the

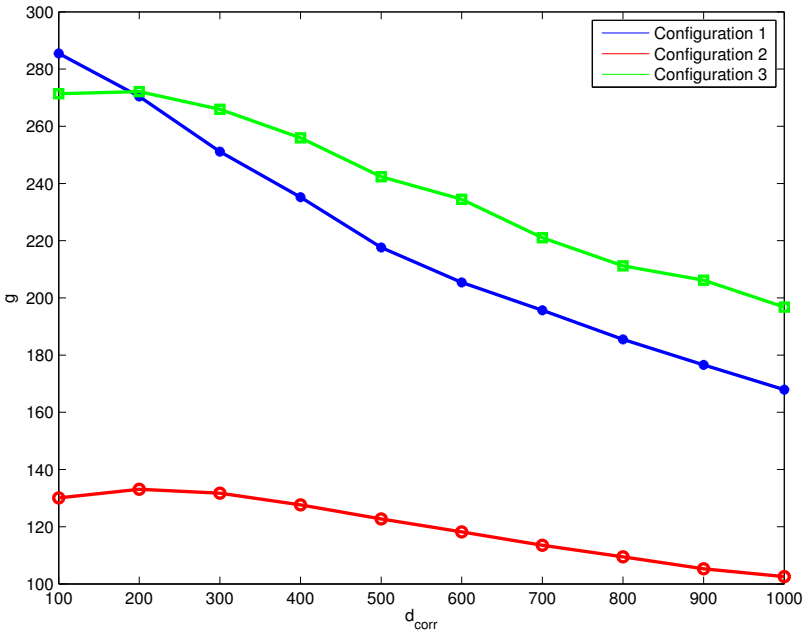

Figure 5.8: Comparison of g for 3 Configurations

circumference of the circle. Calculating g on the circumference of the circle is not possible because CRLB becomes unstable due to the geometry. The value of g rises to infinity as the emitter position approaches the circumference of the sensor circle. Based on this knowledge, the mean of the grid surface is calculated as the mean of all grid points that are not on the circumference of the sensor circle. The mean value of g is 85.7 meters when $d_{corr} = 100m$ and 56.9 meters when $d_{corr} = 1000m$. Fig. 5.11 compares the value of $\overline{g}$ for the circle with varying radii. In this case, the optimal circle radius for reducing the average position error in the 1200-by-1200 meter area is 450 meters when $d_{corr} = 1000m$ and 600 meters when $d_{corr} = 100m$. The optimal radius is slightly smaller when correlation is high versus when it is low. Also, when the radius of the circle is small, the difference between the two GDOP is larger than when the radius of the circle is larger.

For the second experiment, 9 sensors are positioned in a symmetric 3 by 3 square grid configuration. Fig. 5.12 shows the sensor configuration when the spacing between adjacent sensors in the same row and column is 300, and it also shows the surface of g when $d_{corr} = 100m$ and $d_{corr} = 1000m$. The same 1200-by-1200 meter grid surface as the previous test is used. Fig. 5.12 shows the value of g rises significantly outside the convex hull of the sensor grid. Fig. 5.12 also shows the increase in correlation decreases the difference between the peaks and valleys of the surface. For this experiment, all values of the grid surface are used to compute the average g since there are no points where g cannot be computed. Fig. 5.13 compares the mean values of g with varying sensor grid spacing. The sensor grid spacing is

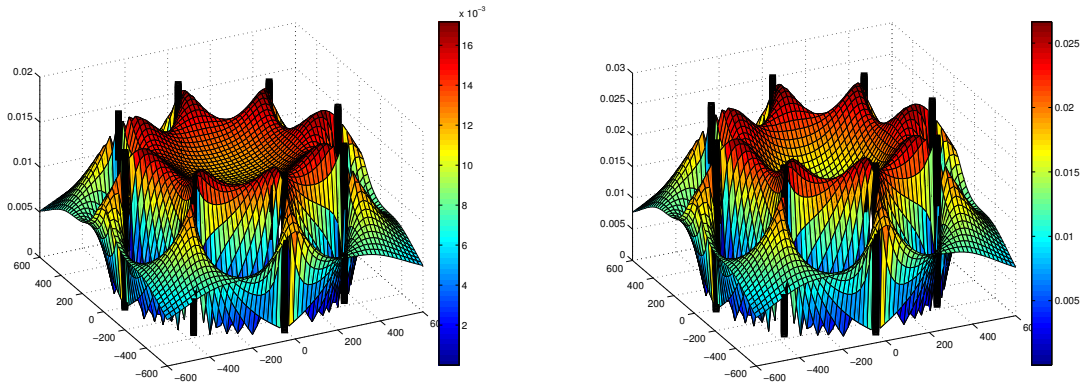

(a) $d_{corr} = 100m$ (b) $d_{corr} = 1000m$

Figure 5.9: Surface of g^{-1} for Circle Configuration. The black lines are the fixed sensor positions.

defined as the distance between any two adjacent sensors in the same row or column. In this case, the optimal sensor spacing is 350 meters when $d_{corr} = 1000m$ and 400 meters when $d_{corr} = 100m$. For this scenario, similar to the previous test with the circle, the optimal configuration when the correlation is high is slightly more compact than when correlation is low.

For the third experiment, 8 sensors are randomly positioned within a square box centered at [0,0], and the emitter is randomly positioned within a different square box centered at [0,0] and with sides of length 2000 meters. The length of the sides of the sensor box range from 800 to 3000 meters. 10,000 trials are conducted for each sensor box size. A single trial consists of a random set of sensors and emitter drawn from their respective boxes, and the calculated g. Fig. 5.14 shows the average value of g from the 10,000 trials for each of the sensor box sizes. When $d_{corr} = 100m$, the optimal sensor box size is 2600 meters, when $d_{corr} = 1000m$, the optimal sensor box size is 2000 meters.

All three experiments show that the optimal sensor configuration for the 1200-by-1200 meter area gets smaller as the correlated shadowing is increased.

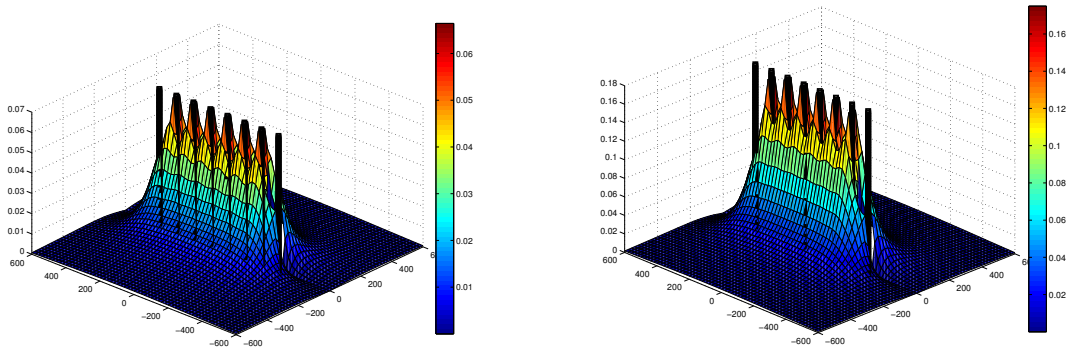

(a) $d_{corr} = 100m$ (b) $d_{corr} = 1000m$

Figure 5.10: Surface of g^{-1} for Line Configuration. The black lines are the fixed sensor positions.

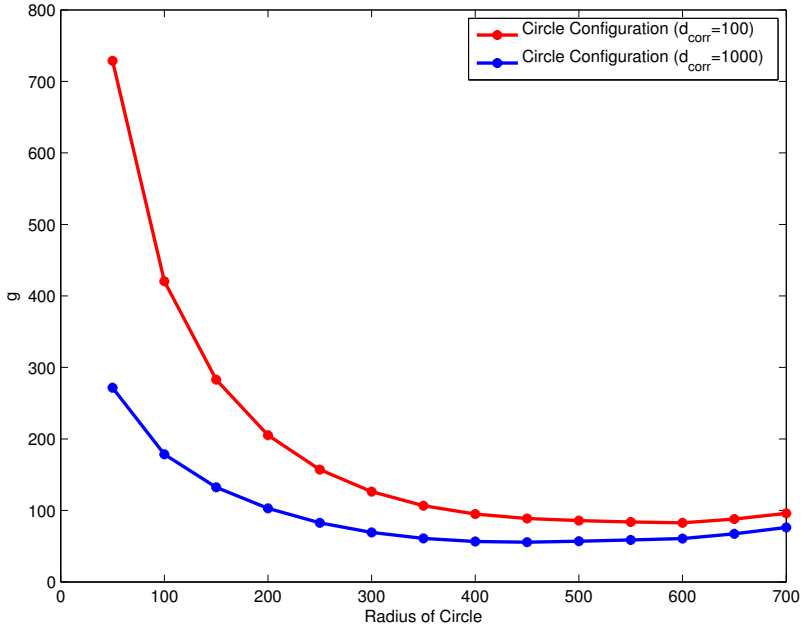

Figure 5.11: Comparison of Mean g for Circle Configuration with Changing Radius

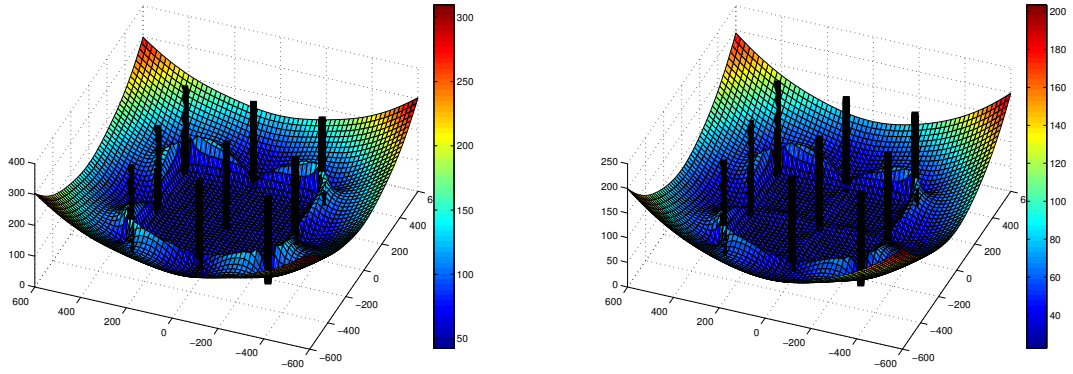

(a) $d_{corr} = 100m$ (b) $d_{corr} = 1000m$

Figure 5.12: Surface of g for Grid Configuration. The black lines represent the fixed sensor positions.

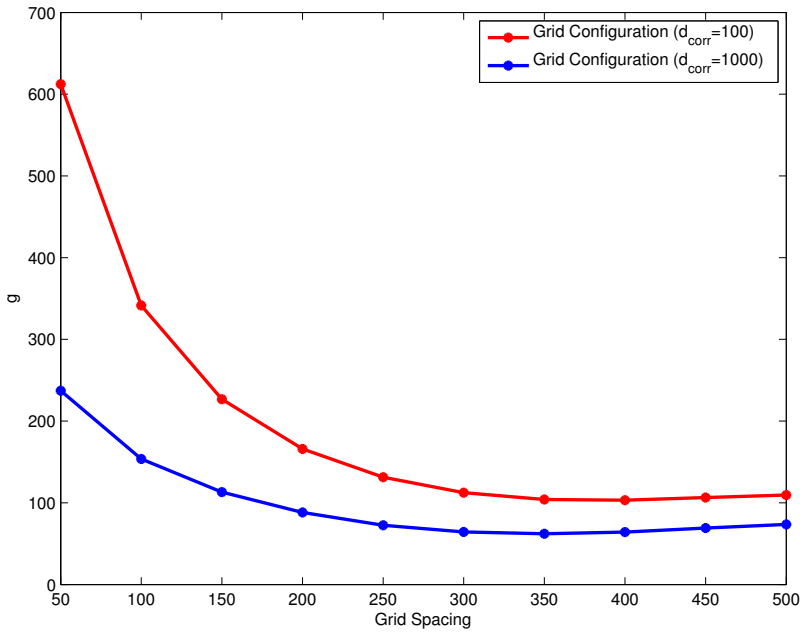

Figure 5.13: Comparison of Mean g for Grid Configuration with Varying Grid Spacing

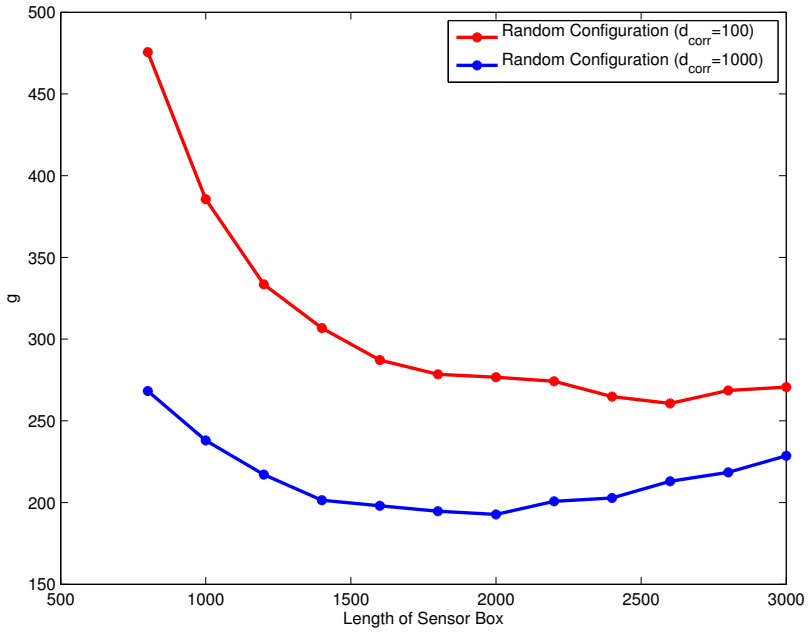

Figure 5.14: Comparison of Mean g for Random Configuration with Varying Sensor Box Size

Chapter 6

New Objective Functions

6.1 Definition and Theory

A new objective function for DRSS-based localization is presented in this section. The DRSS-based localization methods presented so far include the NLSD estimator (Eqn. 3.4) and the ML estimator with independent difference pairs (Eqn. 5.10). An ideal NLSD estimator would be weighted by the variance as follows [32]:

$$\hat{\boldsymbol{\theta}} = \arg\min_{\boldsymbol{\theta}} \sum_{i=1}^{N-1} \sum_{j=i+1}^{N} \frac{1}{\sigma_{ij}^2} \left(\Omega_i - \Omega_j - 10\alpha \log_{10} \left(\frac{d_j}{d_i} \right) \right)^2 \tag{6.1}$$

In this formulation, the difference pairs with the higher variance are given less weight than the difference pairs with lower variance. If the variances are all equal or unknown, then the function reduces to the original NLSD estimator in Eqn. 3.4. In this paper, it is assumed the variance σ_i^2 between the emitter and sensor i is equivalent to the variance between the emitter and any other sensor j. Specifically, $\sigma_j^2 = \sigma_i^2 \forall i, j$. Assuming this, the variance for any difference pair is $\sigma_{ij}^2 = 2(1 - \rho_{ij})\sigma_x^2$, where $\sigma_x^2 = \sigma_i^2 = \sigma_j^2$. If this definition of variance is used, Eqn. 6.1 becomes the following:

$$\hat{\boldsymbol{\theta}} = \arg\min_{\boldsymbol{\theta}} \sum_{i=1}^{N-1} \sum_{j=i+1}^{N} \frac{1}{(1 - \rho_{ij})} \left(\Omega_i - \Omega_j - 10\alpha \log_{10} \left(\frac{d_j}{d_i} \right) \right)^2 \tag{6.2}$$

With this formulation, knowledge of σ_x is not required. This is a practical result because in reality, it is difficult to determine σ_x. The value of ρ_{ij} can be estimated using the model in Eqn. 2.6 where it is solely dependent upon the distance between two sensors. In this case, the knowledge of d_corr must exist or it must be estimated. This objective function in Eqn. 6.2 will be referred to as the non-linear least squares weighted DRSS (NLSWD) estimator.

An alternate NLSWD estimator is as follows:

$$\hat{\boldsymbol{\theta}} = \arg\min_{\boldsymbol{\theta}} \sum_{i=1}^{N-1} \sum_{j=i+1}^{N} \rho_{ij} \left(\Omega_i - \Omega_j - 10\alpha \log_{10} \left(\frac{d_j}{d_i} \right) \right)^2 \tag{6.3}$$

This formulation of the NLSWD estimator is identical to original, except the weight is ρ instead of $\frac{1}{(1-\rho)}$. The two weights serve similar functions by weighting the residuals with higher variance lower than the residuals with lower variance, but the values of the weights are drastically different. The weight of $\frac{1}{(1-\rho)}$ applies an exponential transformation to the value of ρ. The estimator in Eqn. 6.3 is denoted as NLSAD in this paper.

6.2 Simulation Analysis

This section compares the performances of the NLSD, NLSWD, NLSAD, and the MLER estimators. The performances of the NLSD and NLSR estimators are compared in Chapter 4 and are found to be very similar. The performance is tested using the same simulated RSS values based on Eqn. 4.1 and the process outlined in Chapter 4. The average miss distance is determined by averaging the miss distances for 4000 trials. For each trial, a set of sensors and one emitter are randomly positioned in a 1000-by-1000-meter square box. Fig. 6.1 shows the results of the estimators from tests ranging from 4 to 16 sensors. The average of the average miss distances for 4 to 16 sensors for each estimator is given in Table 6.1. The performances are very similar when d_{corr} is low, but the MLER estimator clearly outperforms the others when d_{corr} is high. This result is expected because the MLER estimator fully accounts for all of the correlated shadowing information. And as shown in Chapter 5, the MLER estimator is optimal and nearly achieves the CRLB. The performance increase of the weighted DRSS estimators over the standard DRSS estimator is minimal.

Table 6.1: Average Performance for 4-16 Sensors

Estimator	$d_{corr} = 150m$ (m)	$d_{corr} = 600m$ (m)
NLSD	251.3	207.1
NLSWD	250.4	202.5
NLSAD	242.2	202.9
MLER	239.7	179.7

In the previous experiment, perfect knowledge of d_{corr} is used for the estimators. A second round of tests is performed to evaluate the impact of imperfect knowledge of d_{corr} on the average miss distance. In this test, 10 sensors are randomly positioned in a 1000-by-1000 meter square box for 4000 trials. Fig. 6.2(a) shows the results from a test where the actual value of $d_{corr} = 150m$ and the value of d_{corr} used with the estimators ranges from 50 to

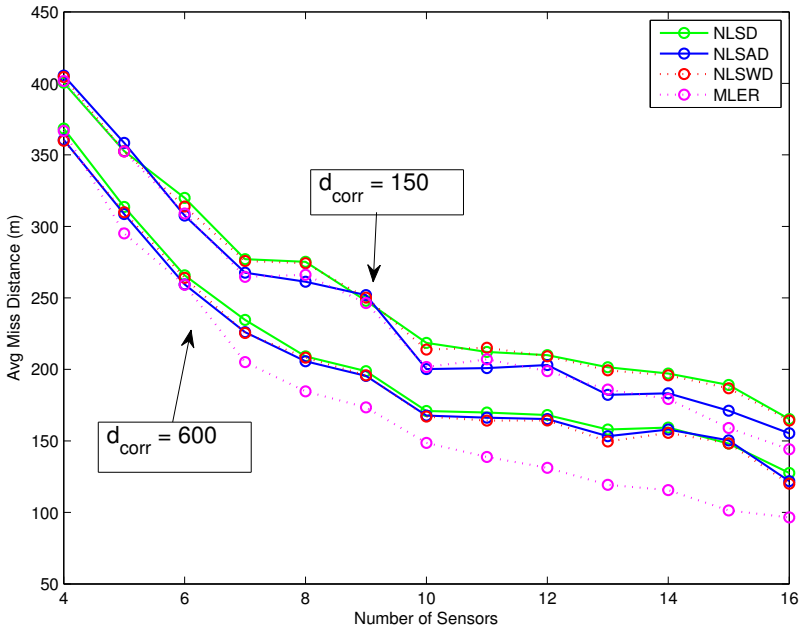

Figure 6.1: Performance Comparison of Estimators

800 meters. Fig. 6.2(b) shows similar results except the actual value of $d_{corr} = 600m$. The MLER estimator is nearly always the optimal estimator even when imperfect knowledge of d_{corr} is used. Table 6.2 contains the average performance for each estimator for all of the estimated d_{corr} values. Here it is evident, the MLER estimator outperforms the three other estimators when the estimated d_{corr} value varies from 50 to 800 meters. Interestingly, the estimated value of d_{corr} that results in the lowest average miss distance is not necessarily the actual value of d_{corr}.

Table 6.2: Average Performance for Estimated $d_{corr} = 50$ to 800 m

Estimator	Actual $d_{corr} = 150m$ (m)	Actual $d_{corr} = 600m$ (m)
NLSD	218.5	170.9
NLSWD	219.5	170.8
NLSAD	216.2	170.5
MLER	204.9	156.5

6.3 Special Sensor and Emitter Geometry

Section 6.2 evaluated the estimators with the emitter and sensors randomly positioned in a box. This section presents the case where the emitter position is fixed at the center of the box and the sensors are randomly placed in the box. The experiment consists of 4000 trials and the average miss distance is the average error from all trials. Fig. 6.3 compares the performance of the estimators for 4 to 16 sensors. For this sensor configuration, the NLSAD estimator is the best performing estimator when d_{corr} is 150 meters.

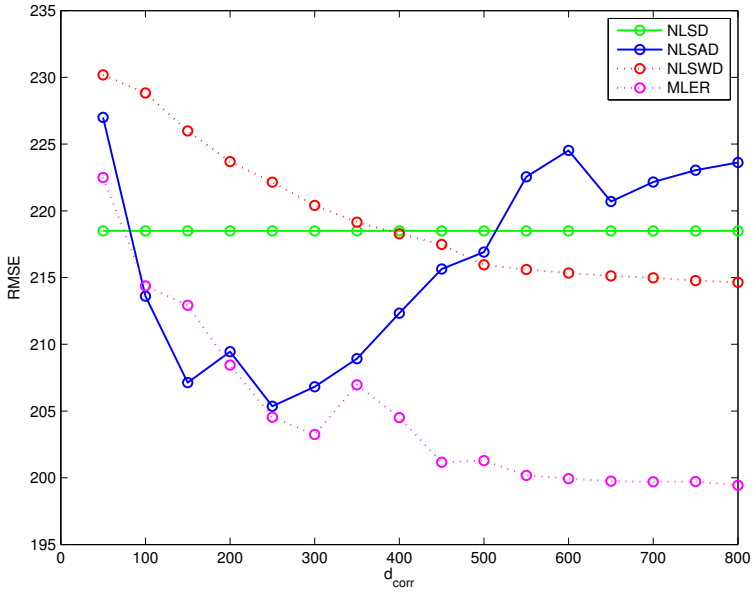

(a) Actual $d_{corr} = 150m$

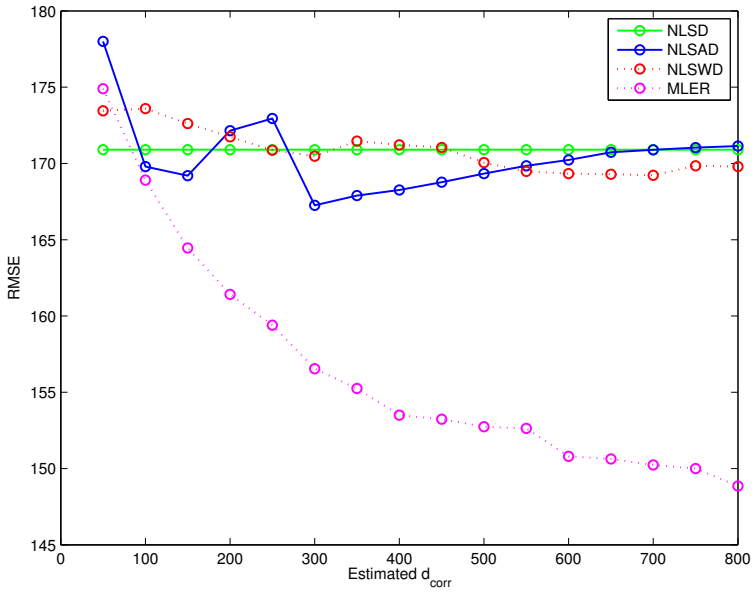

(b) Actual $d_{corr} = 600m$

Figure 6.2: Performance Comparison of Estimators with Imperfect Knowledge of d_{corr}

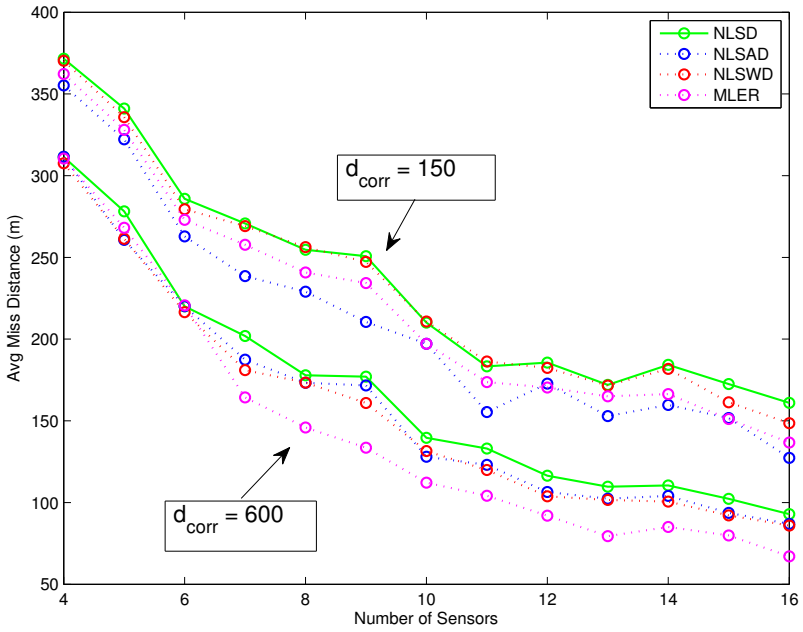

Figure 6.3: Performance Comparison of Estimators when Emitter is Fixed and Centered

Chapter 7

Measurement Campaign

7.1 Overview

The purpose of this measurement campaign is to obtain a set of actual RSS values that can be used to compare the RSS-based localization methods discussed in this paper. Rather than rely on the statistical log-distance model with log-normal shadowing to generate RSS values, actual RSS values and sensor coordinates can be used. The results will also be used to validate the log-distance model (Eqn. 5.4, and the spatially correlated shadowing model (Eqn. 2.6). This chapter details the procedure for obtaining the measurements and analysis of the results.

The localization methods being evaluated rely on a distributed network of sensors that measure RSS from a single emitter at a given time t_x. The number of sensors in the network can range from 4 to more than 25. To reduce the cost of the measurement campaign, only one sensor is used to evaluate RSS at different locations. That is, the measured RSS from a single transmitter is measured by a single receiver that is moved around to several locations. The receiver is mounted to either a bicycle or a car and measurements are taken continuously as the receiver is in motion. The effects of multipath are averaged over a distance of approximately 50 wavelengths, which is sufficient to obtain a measurement of the local mean power due to slow fading (shadowing). Sources [5] and [7] perform similar measurement campaigns that assume averaging RSS over this distance gives an accurate estimate of the shadowing. Since the measurements are based on shadowing effects, it is a valid to assume that RSS measurements at different locations $[X_1, X_2..X_n]$ taken at times $[t_1, t_2...t_n]$ are equivalent to RSS measurements at different locations $[X_1, X_2..X_n]$ taken at a single time t_x. This assumption is made by [25], which states there is no evidence that shadowing significantly changes in time over a fixed path.

Figure 7.1: Field of View to the South of the Transmit Antenna

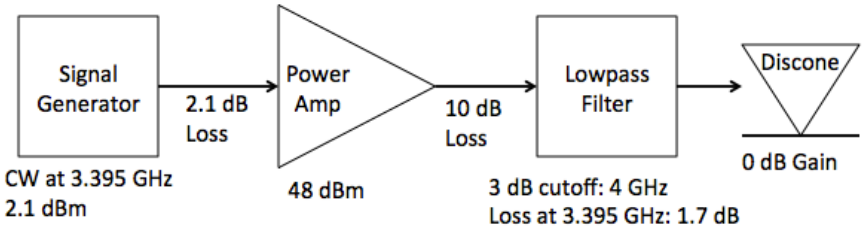

Figure 7.2: Transmitter Block Diagram

7.1.1 Transmitter

Virginia Tech has an FCC license to transmit in the 3.3 to 3.5 GHz spectrum at a maximum ERP of 100 W. This band is classified as a HAM radio band. A survey of the band shows little to no spectral energy aside from environmental and measurement noise. To verify the non-existence of any co-channel interference, the spectrum is evaluated at 3.395 GHz at several locations in the area of interest. The noise floor is calculated to be -125 dBm over a bandwidth of 1 kHz.

The transmit antenna is located on the roof of Durham Hall on Virginia Tech's campus; the exact coordinates of the antenna are 37.2317543 W, -80.4234772 N. The antenna is a monocone that was constructed in Virginia Tech's MPRG lab. It has an omni-directional antenna pattern and operates over a wide bandwidth. The VSWR at 3.395 GHz is 1.55:1 and the return loss is 13.38 dB. Fig. 7.1 shows a panoramic photo of the field of view from the transmit antenna's perspective. The transmit path of the antenna is shadowed to the North by a wall and is shadowed in nearly all other directions from the ground by campus buildings. From bearings 020° T to 080° T, the antenna has a few LOS paths to the ground.

A continuous wave (CW) tone at 3.395 GHz is generated by a signal generator and passed to through a 48 dB power amplifier. Before the signal is transmitted, it is passed through a lowpass filter to reduce spectral content created by the power amplifier. A block diagram of the setup is given in Fig. 7.2.

Table 7.1: RF Hawk Spectrum Analyzer Settings

Setting	*Value*
HREF	-50 dBm
Pre-amp	On
RBW	10 Hz
Measured BW	1 kHz
Center Frequency	3.395 GHz

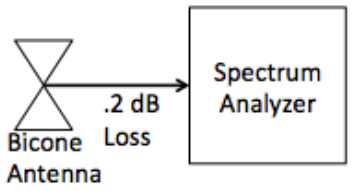

Figure 7.3: Receiver Block Diagram

7.1.2 Receiver

The receiver consists of an antenna and mobile spectrum analyzer. The antenna is a bicone manufactured by Electro-Metrics (model number EM-6865) with 0 dB gain over an isotropic radiator. The coaxial cable connecting the antenna to the spectrum analyzer has a loss of 0.2 dB. The spectrum analyzer is the Tektronix SA2600 RF Hawk. It has a built-in GPS receiver, which makes it capable of automatically logging the geographic position associated with each channel power measurement. The GPS a typical horizontal position accuracy of less than 9 meters. A block diagram of the receiver is given in Fig. 7.3. The RF Hawk is configured with settings listed in Table 7.1.

The receiver is mounted to a bicycle and to a car; the measurements from both are combined. The bicycle allows for measurements to be taken on sidewalks and closer to and between buildings.

7.2 Determining Reference Power

The log-distance model is used to to evaluate the the path loss measurements. This section describes the method to determine the values of c and d_0 in the log-distance model,

$$\Omega_k = c - 10\alpha log_{10}\left(\frac{d_k}{d_0}\right) \tag{7.1}$$

where Ω_k is the received power at distance d_k, and c is the power received at a close distance

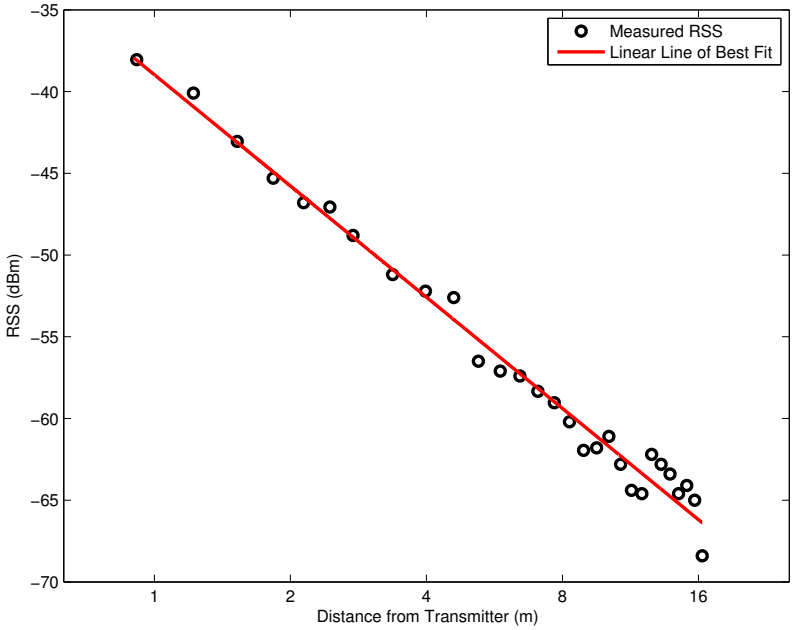

Figure 7.4: RSS at a Close Range with Line of Sight

d_0. The value for c encompasses the losses from the signal generator to the spectrum analyzer due to the coaxial cables and the antennas combined with the power radiated.

Ω_k is measured by placing the receive antenna 3 feet from the transmit antenna at the same elevation and then progressively moving it to a distance of 53 feet. These measurements are conducted with the signal generator set to a power of 14.9 dBm and the power amplifier is removed. The results are plotted in Fig. 7.4. A linear line of best fit is computed and the slope is 2.2686, which is close to the theoretical value of 2. Using any point on the line of best fit, the reference power, c, is selected to be -38.05 dBm with a corresponding d_0 of 3 feet. Since the measurements were conducted without the power amplifier, the value of c is adjusted to $-38.05 + 48 - (14.9 - 2.1) = -2.85$ dBm. This value is used for the remainder of the analysis and is denoted as $c_a = -2.85$.

7.3 Analysis of Measurements

An RSS measurement Ω_i has a coordinate position defined as (x_i, y_i). The local mean power, LP_i, is defined as

$$LP_i = mean(A_i) \tag{7.2}$$

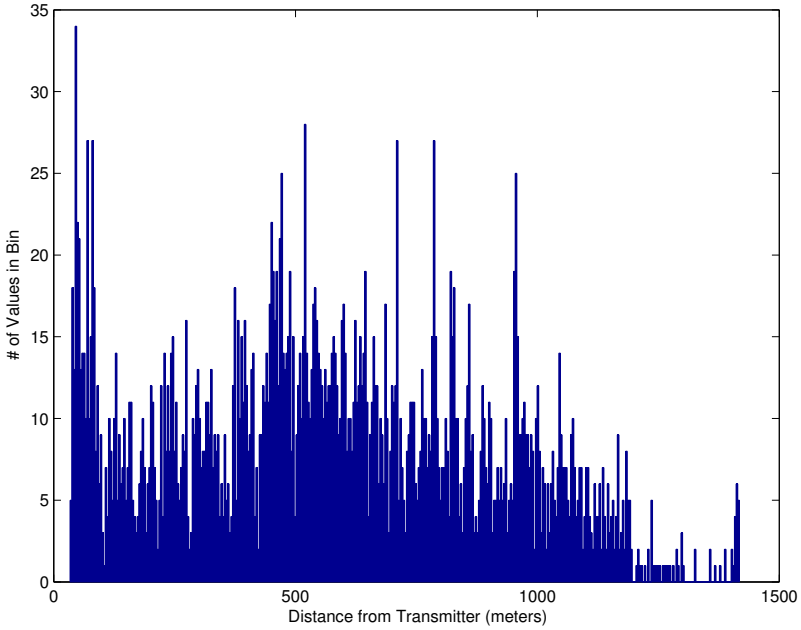

Figure 7.5: Distribution of the Distances Between the Measurement Locations and the Transmitter

where A_i is the set of all Ω that are within a 4-meter radius of Ω_i. And LP_i has same position as Ω_i. Any duplicates in the set of $[LP_i, (x_i, y_i)]$ are removed leaving just one of the duplicate local mean powers. Unless stated otherwise, the rest of the analysis in this paper is on the local mean powers, LP, and will be referred to as the measurements.

The measurements are confined to the Virginia Tech campus and the town of Blacksburg. The maximum distance from the transmitter is 1.42 kilometers. The distribution of the distances between the measurement locations and the transmitter is shown in Fig. 7.5.

A heat map of the measurements is shown in Fig. 7.6. The measurements in the LOS region of the antenna are significantly higher than the measurements in the NLOS regions. Fig. 7.7 compares the received power to distance, and the log-distance model is applied and plotted as well. The path loss exponent, α, is calculated to be the value that reduces the RMSE between the model and the measurements,

$$\hat{\alpha} = \arg\min_{\alpha} \sum_{i=1}^{M} \left(LP_i - c_a + 10\alpha log_{10}\left(\frac{d_i}{d_0}\right)\right)^2 \tag{7.3}$$

where M is the total number of local power measurements and d_i is the distance from the transmitter. α is calculated to be 3.25. The difference between the log-distance model and

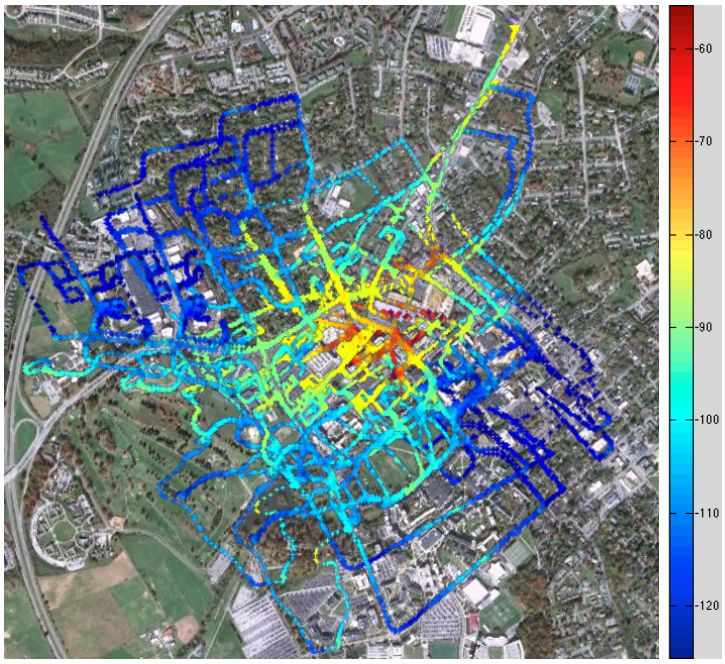

Figure 7.6: Heat Map of RSS Measurements

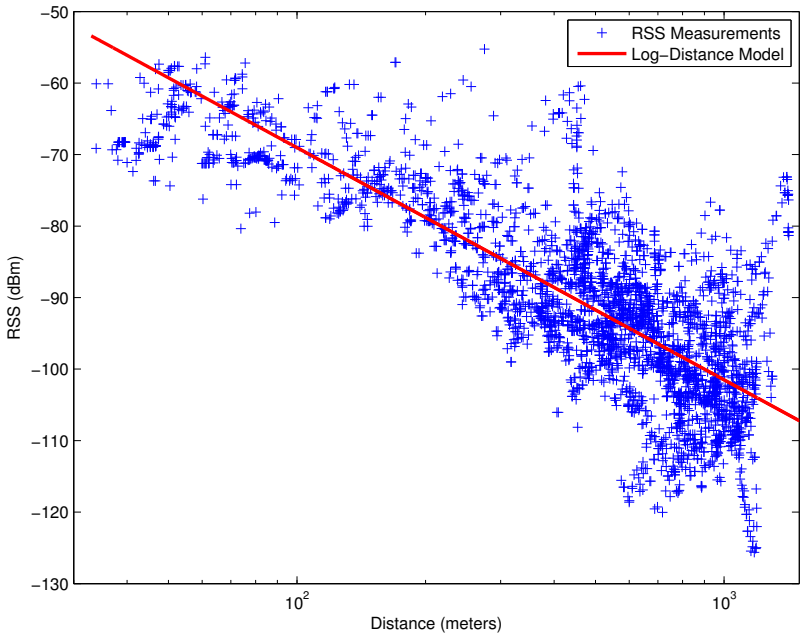

Figure 7.7: RSS Versus the Distance from the Transmitter

the measurements, E, is due to shadowing and is defined as follows:

$$E_x = LP_x - c_a + 10\alpha \log_{10}(\frac{d_i}{d_0}) \tag{7.4}$$

Source [23] shows these errors should follow a log-normal distribution with zero mean, and a variance, σ_x^2. The normalized empirical distribution of E is shown in Fig. 7.8(a). The mean is 0.12 dBm and the σ_x^2 is 69.54 dB. Fig. 7.8(a) also shows a Gauss distribution with zero mean and $\sigma_x^2 = 69.54$. From this view, it is evident the empirical distribution is skewed to the right and is not a perfect Gauss distribution. Table 7.2 shows the theoretical Gauss distribution fitted to the observed frequencies of E. Using the chi-square goodness-of-fit test, the null hypothesis that the vector E is a random sample from a normal distribution, is rejected at the 99% significance level. The Kurtosis value of the distribution is 1.31 (a normal distribution has a value of 0). The standard error of Kurtosis with 3236 RSS measurements is approximately $\sqrt{\frac{24}{3236}} = .0861$ [26]. The value 1.31 is well beyond two standard errors of Kurtosis. Since the Kurtosis value is positive, the distribution is leptokurtic, meaning that the peak is too tall.

The n Gauss shadowing variables associated with the links from the emitter to each sensor can be defined by an $n \times n$ covariance matrix, $\mathbf{\Gamma}$. Source [7] shows the correlation between two links is dependent upon the distance between the two sensors. As the distance between two sensors decreases, the statistical correlation between the two shadowing variables increases. Fig. 7.8(b) illustrates the E at each measurement location. From Fig. 7.8(b), it is evident that spatial correlation exists because the errors tend to be grouped together in groups of similar error. One model for spatial correlation is given in [34] where an off-diagonal element, (i, j) of $\mathbf{\Gamma}$ is defined as follows:

$$\mathbf{\Gamma}_{(i,j)} = \sigma_x^2 \exp\left(-\frac{d_{ij}}{d_{corr}} \ln(2)\right), \;\; i \neq j \tag{7.5}$$

where d_{ij} is the distance between sensors i and j, and d_{corr} is a constant correlation distance, which is based on the distance at which the correlation ρ drops to 0.5.

In order to verify Eqn. (7.5), the distance where ρ drops to 0.5 is determined. The set $S_{v,r}$ is defined as follows:

$$S_{v,r} = [(E_j^{(0)}, E_k^{(0)}), (E_j^{(1)}, E_k^{(1)}), ..., (E_j^{(M-1)}, E_k)^{(M-1)}] \tag{7.6}$$

is the set of all unique pairs of (E_j, E_k) where $v < d_{jk} < v + r$ and $j > k$. And $d_{jk} = \sqrt{(x_k - x_j)^2 + (y_k - y_j)^2}$. The set $S_{v,r}$ is sorted by d_jk and then broken up into 50 equal subsets, $S_{v,r} = [S_{v,r}^{(0)}, S_{v,r}^{(1)}, ..., S_{v,r}^{(49)}]$.

The correlation coefficient is defined using the sample Pearson correlation coefficient and $\rho_{v,r}$ is the correlation of the set $S_{v,r}$:

$$\rho_{v,r} = \frac{1}{50} \sum_{j=0}^{49} \rho_{v,r}^{(j)} \tag{7.7}$$

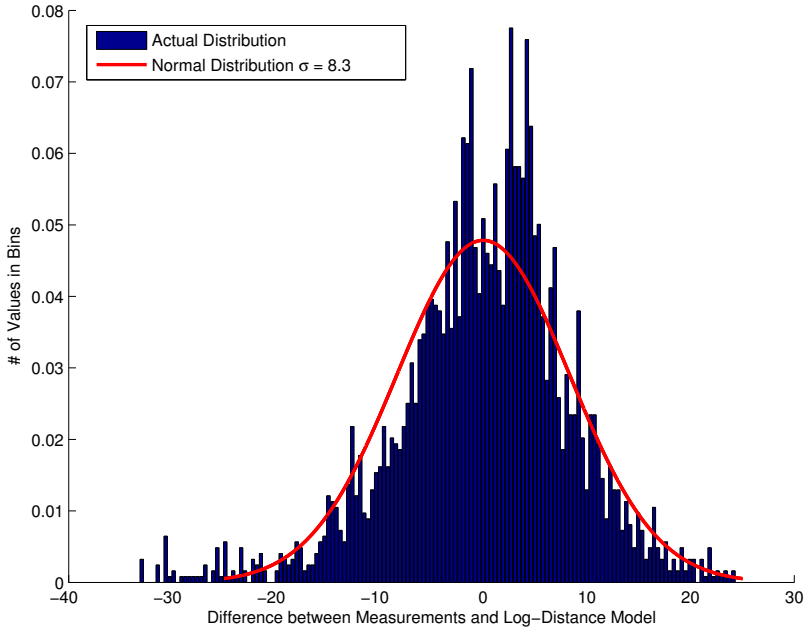

(a) Normalized Empirical Distribution of E and Theoretical Gauss Distribution ($\sigma = 8.3$)

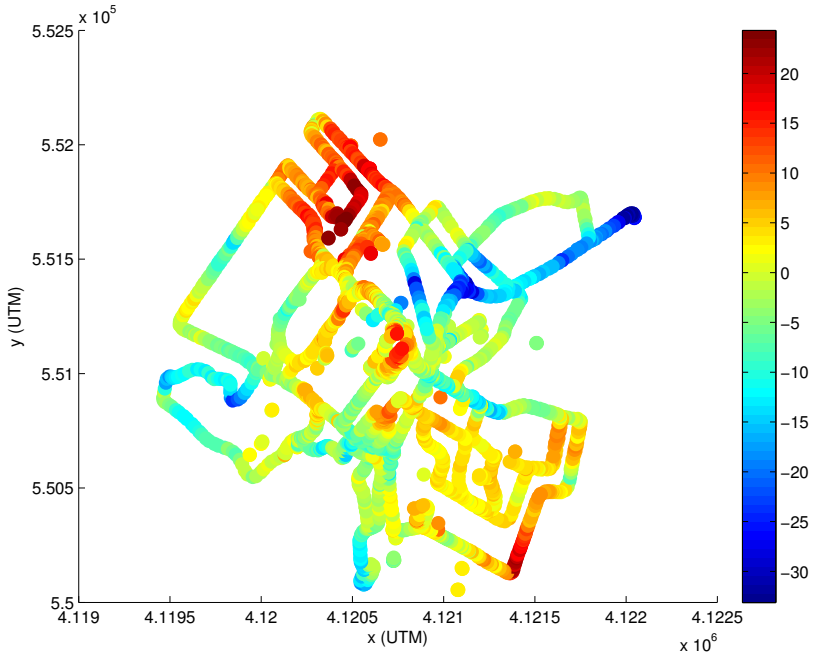

(b) Heat Map of E

Figure 7.8: Probability and Distribution of E.

Table 7.2: Theoretical Normal Distribution Fitted to Observed Frequency

Class Limit X	$x = \frac{X-.12}{8.33}$	P($\leq x$)	Difference	3236 x Difference = theoretical frequency	Observed Frequency
-36	-4.09	0			
			.00009	.29124	17
-31	-3.52	.00009			
			.00077	2.4917	18
-26	-2.96	.00086			
			.00476	15.403	35
-21	-2.39	.00562			
			.02086	67.503	59
-16	-1.82	.02468			
			.06447	208.62	172
-11	-1.26	.09095			
			.14031	454.04	344
-6	-.693	.23126			
			.21526	696.58	653
-1	-.127	.44652			
			.232280	753.34	852
4	.439	.67932			
			.17747	574.29	641
9	1.01	.85679			
			.09538	308.65	281
14	1.57	.95217			
			.03612	116.88	126
19	2.14	.98829			
			.00964	31.195	38
24	2.70	.99793			
			.00181	5.8572	0
29	3.26	.99974			
			Total	3235.2	3236.0

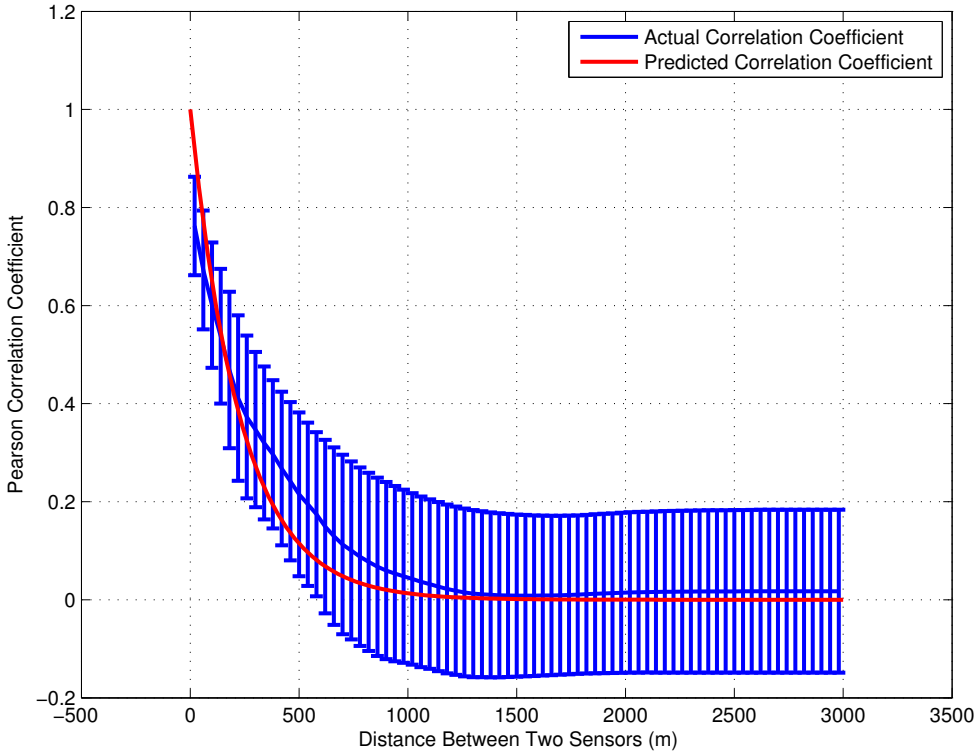

Figure 7.9: Spatial Correlation of E Based on Eqn. 7.7 and Theoretical Correlation Based on Eqn. 2.6 ($d_{corr} = 160m$)

And

$$\rho_{v,r}^{(j)} = \frac{\sum_{i=0}^{M-1}(E_j^{(i)} - \overline{E_j})(E_k^{(i)} - \overline{E_k})}{\sqrt{\sum_{i=0}^{M-1}(E_j^{(i)} - \overline{E_j})^2}\sqrt{\sum_{i=0}^{M-1}(E_k^{(i)} - \overline{E_k})^2}} \tag{7.8}$$

where $\overline{E_j} = \frac{1}{M}\sum_{i=0}^{M-1} E_j^{(i)}$, $\overline{E_k} = \frac{1}{M}\sum_{i=0}^{M-1} E_k^{(i)}$ and M is the number of (E_j, E_k) pairs in $S_{v,r}^{(j)}$. Fig. 7.9 shows the calculated $\rho_{v,r}$ based on Eqn. 7.7 when v is the vector $[0, 40, 80...3000]$ and $r = 40$. Based on these results, the value for d_{corr} is ≈ 160 meters.

Chapter 8

Experimental Evaluation of Location Estimators

The measurements obtained in Chapter 7 are now used to evaluate the location estimators. Each LP_i is assumed to be a realization of a sensor position and measured RSS. A database of LPs and their positions is created to ensure experiments are repeatable on the same set of measurements. To create the database, LPs and corresponding positions are uniformly selected from the data set. A set of 16 LPs and positions are placed in each row of the database. Each row represents an independent trial. So a single trial with 6 sensors uses the first 6 LPs and positions in the first row of the database. The database is structured as shown in Table 8.1.

Table 8.1: Structure of Sensor Database

Trial	Sensor 1 RSS	Sensor 1 Position	Sensor 2 RSS	Sensor 2 Position	...
1	LP_i	(x_i, y_i)	LP_j	(x_j, y_j)	...
2	LP_k	(x_k, y_k)	LP_m	(x_m, y_m)	...
...	...	...	...	...	...
N	LP_n t	(x_n, y_n)	LP_t	(x_t, y_t)	...

It should be noted that because the measurement campaign was conducted with one emitter at a fixed location, the average performance of the estimators will most likely be better than the performance of the estimators in practice. As shown in Chapter 5, this geometry has a significantly lower average miss distance than when the emitter is randomly positioned as well as the sensors.

8.1 Comparing Theoretical and Actual RSS

This sections compares the performance of the estimators using simulated RSS values versus the estimators using actual RSS values. The simulated RSS values are generated using Eqn. 4.1 with the following parameters: σ^2= 69.54 dB, mean = 0, d_{corr}= 160 meters, α=3.25. These parameters are equivalent to the empirical characteristics of the measurements as detailed in Chapter 7. The simulated RSS values are generated at the same positions as the corresponding actual RSS values. The only difference between the simulated and actual RSS results is that the simulated RSS comes from a perfect Gauss distribution. The miss distances for each estimator from 3000 trials are averaged and shown in Fig. 8.1. The CRLB is calculated using the same sensor positions as the trials and averaged across all trials. The difference between the average miss distances for an estimator using simulated RSS versus actual RSS is small. Table 8.2 shows the average of the average miss distances for 4 to 16 sensors for each of the estimators. This small difference between the estimators using theoretical and actual RSS helps to validate the theoretical models for RSS.

The theoretical results are superior than the actual results for all estimators except the NLSAD. This is due to the fact that the theoretical RSS values are drawn from an ideal distribution. The maximum separation in average miss distances between an estimator based on theoretical RSS versus actual RSS comes from the MLER estimator and is 8.6%. This is expected because the MLER estimator is based on the assumption that the distribution is Gauss and takes full advantage of the information in the covariance matrix. And thus deviations from these assumptions will have a greater effect on the performance of the MLER estimator than the other estimators. This shows that while the MLER estimator performs best in simulation, it may not perform best under actual conditions.

Table 8.2: Average Performance for 4-16 Sensors

Estimator	Theoretical RSS (m)	Actual RSS (m)
NLSD	221.7	230.1
NLSWD	220.6	229.1
NLSAD	196.6	189.4
MLER	216.7	235.3

The NLSAD estimator consistently has the lowest average miss distance for 4 to 16 sensors from both the theoretical and actual RSS values. This is consistent with the results in Chapter 5, which show the NLSAD estimator outperforms the other estimators when correlation is relatively low, and the emitter position is fixed at the center. The results further show that the NLSAD estimator is less effected by imperfect distribution of the actual RSS values. The NLSAD estimator actually performs better with the actual RSS values compared to the theoretical RSS values, while the other estimators are opposite.

The results also show that the CRLB is a good indicator of the expected performance, not only in simulation, but also with actual RSS values. When the number of sensors is high ($>$ 10), the CRLB closely matches the average miss distance of the NLSAD estimator.

8.2 Further Analysis of Estimators using Actual RSS

This section evaluates the effect of imperfect knowledge of d_{corr} on the estimators using actual RSS values. In Chapter 7, d_{corr} of the measurements is estimated to be 160 meters. Section 8.1 evaluated the estimators using this value of d_{corr}. Fig. 8.2 compares the estimators' performance when the estimated d_{corr} ranges from 50 to 800 meters. Table 8.3 shows the average performance for all of the d_{corr} estimates. The NLSAD is nearly always superior to the other estimators, and it has a much lower average miss distance across the range of d_{corr} estimates.

Table 8.3: Average Performance for Estimated d_{corr} of 50 to 800 meters

Estimator	Average Miss Distance (m)
NLSD	219.1
NLSWD	200.7
NLSAD	175.6
MLER	201.2

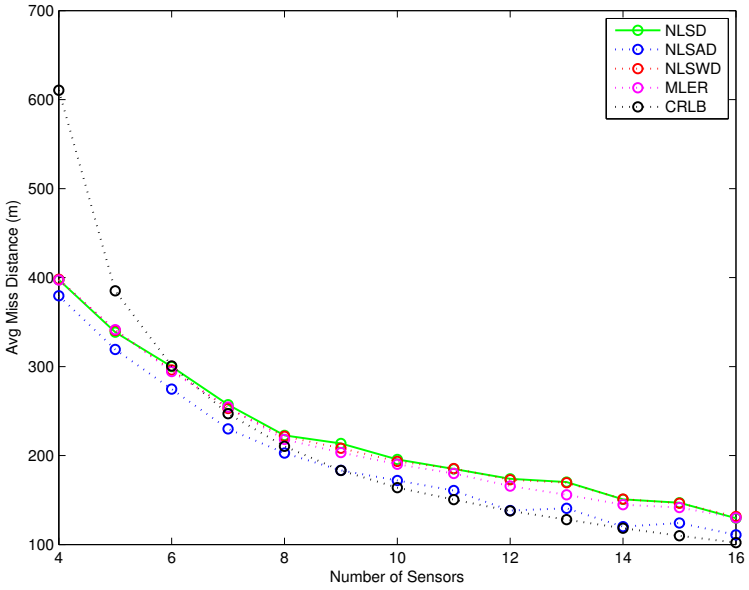

(a) Simulated RSS

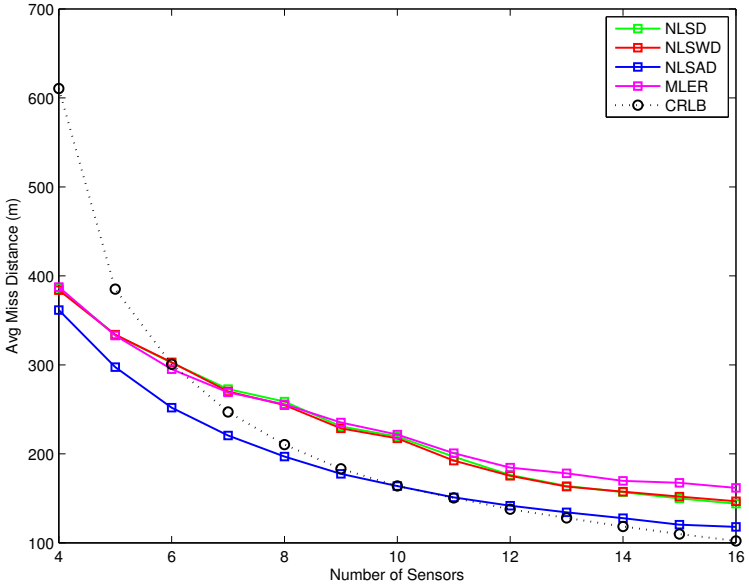

(b) Actual RSS

Figure 8.1: Comparison of Theoretical and Actual RSS

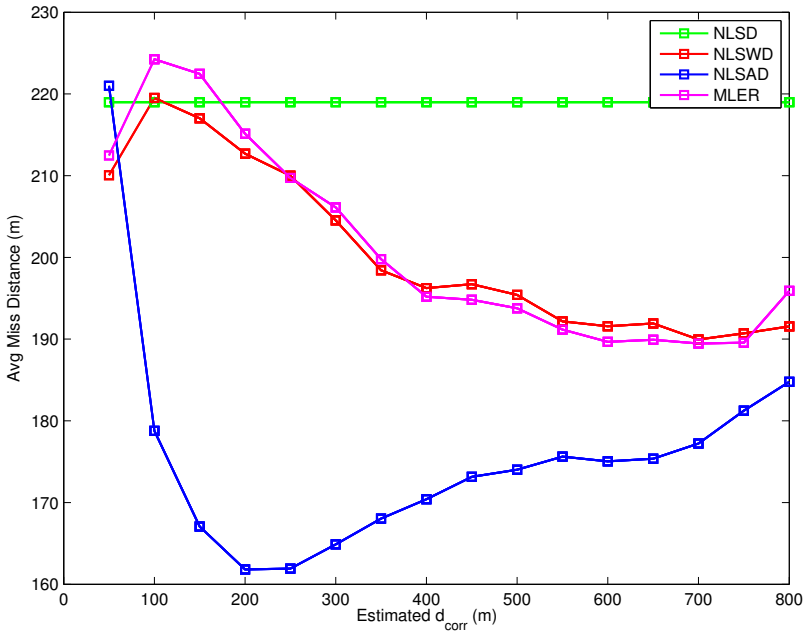

Figure 8.2: Performance of Estimators with Varying Knowledge of d_{corr}. 10 sensors

Chapter 9

Conclusions

RSS-based localization is a promising localization solution for scenarios that involve the localization of non-collaborative emitters. These scenarios include the localization of combative jamming devices, or the localization of legacy systems in the same area as cognitive systems that are seeking open spectrum. RSS-based localization is an ideally suited solution because it needs low network overhead, little knowledge of the emitter's signal, and allows for a diverse set of devices to be used. In this paper, RSS-based localization in the presence of correlated shadowing was examined. The location estimators were examined both in simulation and using an actual set of measurements. A new ML estimator and CRLB were presented that account for spatially correlated shadowing and imperfect knowledge of the emitter's reference power. It was shown that correlated shadowing has a positive effect on the accuracy of an RSS-based location estimator. A list of the major contributions of this paper is given below:

1. This paper presented a new ML estimator and CRLB for RSS-based localization in the presence of correlated and imperfect knowledge of the emitter's reference power.

2. The effects of correlated shadowing on an RSS-based location estimator were thoroughly examined. It was shown that an increase in correlated shadowing will improve the accuracy of an RSS-based location estimator. It was also demonstrated that the ideal sensor geometry which minimizes the average error becomes more compact as correlation is increased.

3. The paper introduced a new DRSS location estimator that uses correlated shadowing information to improve performance. The estimator performed better than the ML estimator when the emitter was at a fixed position and the sensors were randomly placed around it.

4. A measurement campaign was conducted that characterized path loss at 3.4 GHz. The measurements were compared to the log-distance model, and the errors between the

model and the measurements had a Kurtosis value of 1.31. The errors were determined to be spatially correlated with an average correlation coefficient of 0.5 at a distance of 160 meters.

5. The performance of the location estimators in simulation was compared to the performance using measurements from the measurement campaign. The performance was very similar, with the largest differences in the ML estimator. In both cases, the new DRSS estimator outperformed the other estimators and achieved the CRLB.

Bibliography

[1] *Proc. IRE*, volume 34, 1946.

[2] Gps-less low cost outdoor localization for gps-less low cost outdoor localization for very small devices. In *IEEE Personal Communications Magazine*, pages 28–34, Oct 2000.

[3] M. Brunato and R. Battiti. Statistical learning theory for location fingerprinting in wireless lans, 2005.

[4] B. J. Dil and P. J. M. Havinga. Rss-based localization with different antenna orientations. In *Telecommunication Networks and Applications Conference (ATNAC), 2010 Australasian*, pages 13–18.

[5] V. Erceg, L.J. Greenstein, S.Y. Tjandra, S.R. Parkoff, A. Gupta, B. Kulic, A.A. Julius, and R. Bianchi. An empirically based path loss model for wireless channels in suburban environments. *Selected Areas in Communications, IEEE Journal on*, 17(7):1205 –1211, jul 1999.

[6] FCC. Second memorandum opinion and order 10-174.

[7] M. Gudmundson. Correlation model for shadow fading in mobile radio systems. *Electronics Letters*, 27(23):2145 –2146, nov. 1991.

[8] A. Hatami and K. Pahlavan. Qrpp1-5: Hybrid toa-rss based localization using neural networks. In *Global Telecommunications Conference, 2006. GLOBECOM '06. IEEE*, pages 1–5.

[9] S. Kay. *Fundamentals of Statistical Signal Processing: estimation theory*. 1993.

[10] P. Kristalina, W. Wirawan, and G. Hendrantoro. Improved range-free localization methods for wireless sensor networks. In *Electrical Engineering and Informatics (ICEEI), 2011 International Conference on*, pages 1–6.

[11] Peter Dayan L. F. Abbott. The effect of correlated variability on the accuracy of a population code. In *Neural Computation*, 1999.

[12] K. Langendoen and N. Reijers. Distributed localization in wireless sensor networks: a quantitative comparison. In *Computer Networks*, pages 499–518, 2003.

[13] Jeong Heon Lee. *Physical Layer Security for Wirless Position Location in the Presence of Location Spoofing*. PhD thesis, Virginia Tech, Blacksburg, VA, March 2011.

[14] Jeong Heon Lee and R. M. Buehrer. Location estimation using differential rss with spatially correlated shadowing. In *Global Telecommunications Conference, 2009. GLOBECOM 2009. IEEE*, pages 1–6.

[15] Alberto Leon-Garcia. *Probability, Statistics, and Random Processes for Electrical Engineering*. Prentice Hall, 2007.

[16] J. C. Liberti and T. S. Rappaport. Statistics of shadowing in indoor radio channels at 900 and 1900 mhz. In *Proc. IEEE Military Commun. Conf.*, volume 3, pages 1066–1070, 1992.

[17] L. Mailaender. Geolocation bounds for received signal strength (rss) in correlated shadow fading. In *Vehicular Technology Conference (VTC Fall), 2011 IEEE*, pages 1–6, 2011.

[18] R.W. Ouyang, A.K.-S. Wong, Chin-Tau Lea, and V.Y. Zhang. Received signal strength-based wireless localization via semidefinite programming. In *Global Telecommunications Conference, 2009. GLOBECOM 2009. IEEE*, pages 1–6, 2009.

[19] T. Kremenek P. Castro, P. Chiu and R. R. Muntz. A probabilistic room location service for wireless networked environments. In *Proceedings of Ubiquitous Computing*, pages 18–34, 2001.

[20] P. Krishnamurthy P. Prasithsangaree and P. Chrysanthis. On indoor position location with wireless lans. Technical report, Telecommunications Program, University of Pittsburgh, 2002.

[21] N. Patwari and P. Agrawal. Effects of correlated shadowing: Connectivity, localization, and rf tomography. In *Information Processing in Sensor Networks, 2008. IPSN '08. International Conference on*, pages 82–93, 2008.

[22] P. Pivato, L. Fontana, L. Palopoli, and D. Petri. Experimental assessment of a rss-based localization algorithm in indoor environment. In *Instrumentation and Measurement Technology Conference (I2MTC), 2010 IEEE*, pages 416–421.

[23] T. S. Rappaport. *Wireless Communications: Principles and Practice*. Prentice Hall, 1996.

[24] M. Saxena, P. Gupta, and B. N. Jain. Experimental analysis of rssi-based location estimation in wireless sensor networks. In *Communication Systems Software and Middleware and Workshops, 2008. COMSWARE 2008. 3rd International Conference on*, pages 503–510.

[25] S.S. Szyszkowicz, H. Yanikomeroglu, and J.S. Thompson. On the feasibility of wireless shadowing correlation models. *Vehicular Technology, IEEE Transactions on*, 59(9):4222 –4236, nov. 2010.

[26] Fidell L. S. Tabachnick, B. G. *Using multivariate statistics*. Harper Collins, 1996.

[27] K. Tateishi and T. Ikegami. Decision experiment of attenuation constant during location estimation in rssi. In *Parallel and Distributed Computing, Applications and Technologies, 2008. PDCAT 2008. Ninth International Conference on*, pages 431–436.

[28] Benton K. Thompson. Characterizing and improving the non-collaborative and collaborative localization problems. Master's thesis, Virginia Tech, 2011.

[29] R.M. Vaghefi, M.R. Gholami, R.M. Buehrer, and E.G. Strom. Cooperative received signal strength-based sensor localization with unknown transmit powers. volume 61, pages 1389–1403, 2013.

[30] Frank van Diggelen. *A-GPS: Assisted GPS, GNSS, and SBAS*. Artech House, 2009.

[31] Sichun Wang and Robert Inkol. A near-optimal least squares solution to received signal strength difference based geolocation. In *Acoustics, Speech and Signal Processing (ICASSP), 2011 IEEE International Conference on*, pages 2600–2603.

[32] Sichun Wang, Robert Inkol, and Brad R. Jackson. Relationship between the maximum likelihood emitter location estimators based on received signal strength (rss) and received signal strength difference (rssd). In *Communications (QBSC), 2012 26th Biennial Symposium on*, pages 64–69.

[33] Feng Xiufang, Gao Zhanqiang, Yang Mian, and Xiong Shibo. Fuzzy distance measuring based on rssi in wireless sensor network. In *Intelligent System and Knowledge Engineering, 2008. ISKE 2008. 3rd International Conference on*, volume 1, pages 395–400.

[34] E. K. Tameh Z. Wang and A. Nix. Simulating correlated shadowing in mobile multihop relay/ad-hoc networks. Technical report, IEEE 802.16 Broadband Wireless Access Working Group, 2006.

[35] K. Zayana and B. Guisnet. Measurements and modelisation of shadowing cross-correlations between two base-stations. In *Proc. IEEE Int. Conf. Univ. Pers. Comm.*, volume 1, pages 101–105, 1998.